Histopathology

All organs were removed from the mice, fixed with 4% phosphate-buffered formaldehyde (pH 7.2), and prepared for histologic examination. The sections (4 μm in thickness) were stained with hematoxylin and eosin (HE). Histologic grading of inflammatory arthritis was performed according to the methods by Edwards et al[23] as follows: a 1-point score indicates hyperplasia/hypertrophy of synovial cells, fibrosis/fibroplasia, proliferation of cartilage and bone, destruction of cartilage and bone, and mononuclear cell infiltrate. Imaging was analyzed by microscope (BX50, Olympus, Tokyo, Japan) at 20 × 10.70 objective lens. Viewfinder Lite Version 1.0 (Olympus) for image acquisition and Adobe Photoshop CS2 for image processing were used.

Measurement of anti-dsDNA Ab, RF, and CII Ab levels

Anti–double-stranded DNA (dsDNA) Abs, rheumatoid factor (RF), and anti-CII Ab were detected by ELISA as described previously.[11] Briefly, flat-bottom plates (Nalge Nunc International, Roskilde, Denmark) were coated with 1.5 μg/mL of native calf thymus DNA (Life Technologies, Rockville, MD) in buffer containing 0.1 M sodium bicarbonate and 0.05 M citric acid at 4°C overnight. Serum samples were serially diluted (starting at 1:200) and added to the plates for 1 hour of incubation at 37°C. After washing, peroxidase-conjugated goat anti-mouse IgG, or IgM (Southern Biotechnology Associates, Birmingham, AL) was added and incubated for 1 hour at 37°C. Ab binding was visualized using orthophenylenediamine (Sigma Chemical). For the measurement of IgG and IgM RF, human IgG and IgM (Chemicon International, Temecula, CA) were coated onto plates at 10 μg/mL (pH 9.6). The microtiter plate was coated with 100 μL CII antigen solution. After washing 3 times, 100 μL/well of serum samples that had been serially diluted in PBS/Tween 20/1% BSA and control serum samples were added and incubated for 1 hour at 37°C. After washing, peroxidase-conjugated goat anti-mouse IgG (at 1.4 μg/mL, 100 μL/well; Organon Teknika, Durham, NC) was added and incubated for 1 hour at 37°C. A total of 100 μL *o*-phenylenediamine (0.5 mg/mL) dissolved in 0.1 M citrate buffer (pH 5.0) containing 0.012% H_2O_2 was added, and the reaction was stopped using 8 N H_2SO_4 (20 μL/well).

Statistics

The Student *t* test was used for statistical analysis. *P* values greater than .05 were considered significant.

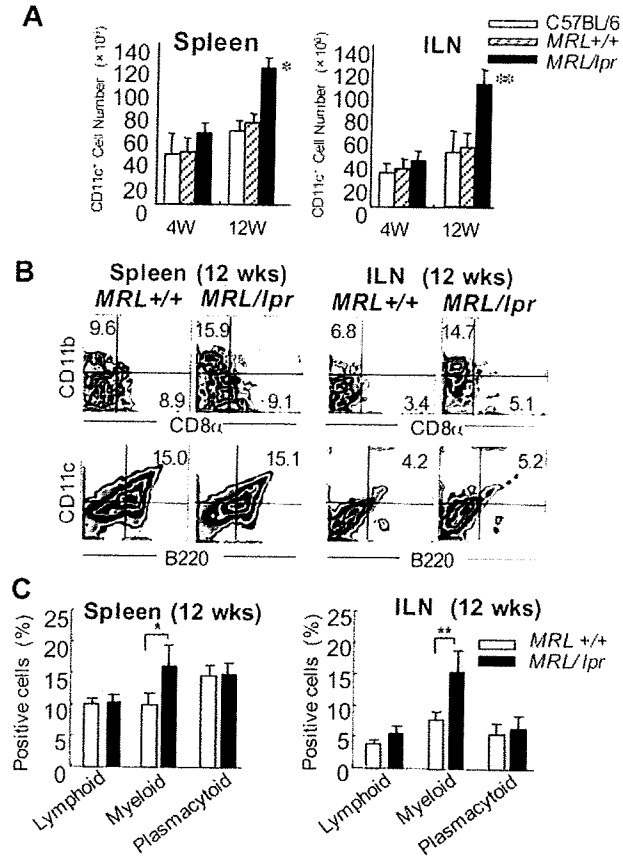

Figure 1. Myeloid dendritic cells in the spleen and inguinal lymph nodes from *MRL/lpr* mice. (A) The CD11c+ DC cell number of the spleen and ILNs is shown as means ± SD of 5 to 7 *MRL/lpr* and control mice at 4 and 12 weeks of age. (B) Mononuclear cells were isolated from the spleen and ILNs at 12 weeks of age, and the proportions were determined using flow cytometry. Shown are representative plots of CD8α+, CD11b+, B220+, and CD11c+ cells. Percentages in each region indicate the frequency of lymphoid (CD11c+CD11b−CD8α+), myeloid (CD11c+CD11b+CD8α−), and plasmacytoid (CD11c+B220+) DCs. Data are representative of 5 to 7 mice in each group. (C) Graph shows the mean frequency of lymphoid, myeloid, and plasmacytoid DCs. *$P > .05$; **$P > .01$ *MRL/lpr* versus *MRL*$^{+/+}$ mice. Results are representative of 3 independent experiments.

Results

DC numbers and subtypes of *MRL/lpr* mice

To examine the number of DCs from *MRL/lpr* mice, the spleen cells and inguinal lymph node (ILN) cells were analyzed at 4 and 12 weeks of age. We found that the DC number of both spleen and ILNs from *MRL/lpr* mice was significantly higher than that from control mice at 12 weeks of age (Figure 1A). We next analyzed the increased subset of DCs from *MRL/lpr* mice. A significant increase of the myeloid ($CD11b^+CD11c^+CD8\alpha^-$) DC subset of both spleen and ILNs from *MRL/lpr* mice was observed in contrast to the population from control *MRL*$^{+/+}$ mice, whereas there was no difference in the lymphoid ($CD11c^+CD11b^-CD8\alpha^+$) and plasmacytoid ($B220^+CD11c^+$) DCs between *MRL/lpr* and control mice (Figure 1B-C). Based on these findings, we recognized the possibility that myeloid DCs from *MRL/lpr* mice may have any influence on the immune disorder of the mice.

Activation of RANKL-stimulated DCs from *MRL/lpr mice*

To determine the function of DCs from *MRL/lpr* mice, we generated BMDCs by using the culture of bone marrow cells with recombinant mouse GM-CSF and IL-4. When the cell-surface markers on BMDCs after the culture for 7 days were determined, the myeloid subset DCs from *MRL/lpr* mice had increased significantly compared with that from *MRL*$^{+/+}$ mice, resembling the phenotype of the spleen and ILN from *MRL/lpr* mice (Figure 2A-B).

Next, activation of the BMDCs from *MRL*$^{+/+}$ and *MRL/lpr* mice stimulated with RANKL or lipopolysaccaride (LPS) was estimated by analyzing the surface phenotypes, including MHC class II, B7.2 (CD86) and B7.1 (CD80). BMDCs were stimulated with 100 ng/mL mouse recombinant RANKL or 100 ng/mL LPS for 48 hours, and then the surface expressions were detected by flow cytometric analysis as shown in Figure 2C. The expressions of MHC class II, B7.1, and B7.2 on BMDCs from *MRL/lpr* mice in response to RANKL were enhanced compared with those from *MRL*$^{+/+}$ mice, but no significant difference in the expressions on the BMDCs stimulated with LPS from between *MRL*$^{+/+}$ and *MRL/lpr* mice (Figure 2C).

This finding indicates that activation of BMDCs from *MRL/lpr* mice via RANKL might be enhanced. In addition, to define the secretion of some cytokines such as IFN-γ, IL-12p40, and IL-10 from RANKL-stimulated BMDCs of *MRL/lpr* mice, BMDCs from

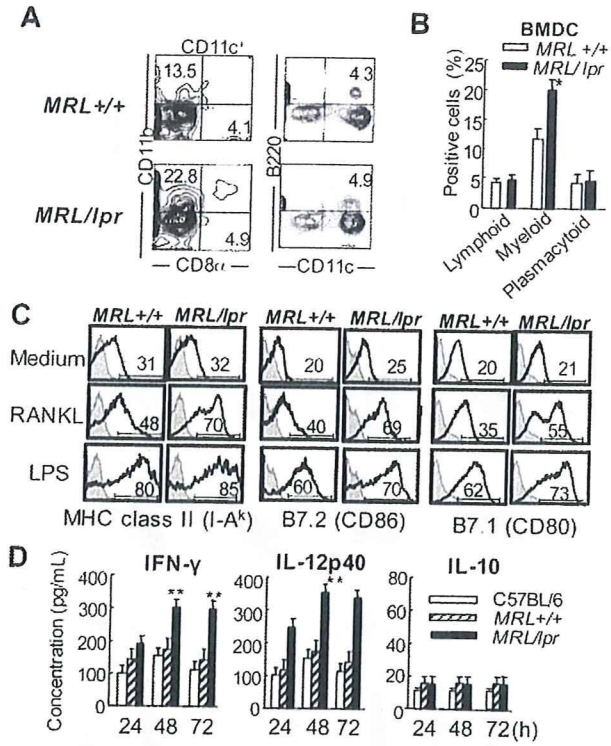

Figure 2. Surface phenotypes and cytokine productions in RANKL-stimulated DCs from *MRL/lpr* mice. (A) BMDCs were generated from *MRL/lpr* and *MRL*$^{+/+}$ mice by using the culture of bone marrow cells with GM-CSF and IL-4 for 7 days; the cell-surface markers of BMDCs were then analyzed. BMDCs from *MRL/lpr* and *MRL*$^{+/+}$ mice were analyzed by flow cytometry. Shown are representative plots of CD8α$^+$, CD11b$^+$, B220$^+$, and CD11c$^+$ cells. Percentages in each region indicate the frequency of lymphoid, myeloid, and plasmacytoid DCs. Results are representative of 3 independent experiments. (B) The graph shows the mean frequency of lymphoid, myeloid, and plasmacytoid DCs. Data are means ± SD of 5 to 7 mice in each group. (C) BMDCs were stimulated with 100 ng/mL mouse recombinant RANKL or 100 ng/mL LPS for 48 hours, and then the surface expressions of MHC class II and costimulatory molecules were detected by flow cytometric analysis. The result is representative of 3 independent experiments. (D) The secretions of IFN-*r*, IL-12p40, and IL-10 in culture supernatants from the BMDCs stimulated by RANKL were detected by ELISA. Data are means ± SD of triplicate samples and are representative of 4 independent experiments. **P* > .05; ***P* > .01, *MRL/lpr* versus control mice.

normal B6 mice, *MRL*$^{+/+}$, and *MRL/lpr* mice were stimulated with RANKL for 24 to 72 hours, and the cytokine secretion of the culture supernatants was analyzed by ELISA. Significantly increased secretions of IFN-γ and IL-12p40, not IL-10, of BMDCs from *MRL/lpr* mice were observed compared with those from C57BL/6 (B6) and *MRL*$^{+/+}$ mice (Figure 2D). These data suggest that the Fas molecule may influence the activation and function of DCs through RANKL signaling.

Signaling molecules of DCs through RANKL

It is well known that the RANK/RANKL pathway includes a lot of signaling molecules.[24,25] Among them, NF-κB plays a key role for DC maturation and activation.[26] NF-κB activation through RANK/RANKL occurs by nuclear translocation following inducible phosphorylation of inhibitory IκB by IKK complex.[27,28] Therefore, IKKα expression and phosphorylation of IκB (p-IκB) in RANKL-stimulated BMDCs from B6, *MRL*$^{+/+}$, and *MRL/lpr* mice were analyzed by Western blotting. In addition, the expression of TRAF6 downstream from RANK in RANKL-stimulated BMDCs from *MRL/lpr* and control mice was determined.

Increasing expression of TRAF6 after stimulation with RANKL was detected in BMDCs from *MRL*$^{+/+}$ mice. In *MRL/lpr* mice, a much higher expression of TRAF6 in the BMDCs was observed in contrast to that of the control mice. In addition, the expression of IKKα of *MRL/lpr* DCs was up-regulated relative to those of B6 and *MRL*$^{+/+}$ DCs (Figure 3A). Notably, the prominent phosphorylation of IκB of *MRL/lpr* DCs was detected compared with that of control DCs parallel with the increased expressions of TRAF6 and IKKα (Figure 3A). Furthermore, nuclear translocation of NF-κB subunits (p65 and p50) of RANKL-stimulated *MRL/lpr* DCs had increased remarkably compared with that of control DCs (Figure 3B). To define the movements of RANKL-mediated signaling molecules of *MRL/lpr* DCs, the expression of each protein was confirmed by confocal microscopic analysis. Consistent with the results of Western blot analysis using the cytoplasmic and nuclear proteins, the increased nuclear translocation of NF-κB and the up-regulated TRAF6 and p-IκB in the cytoplasm from RANKL-stimulated

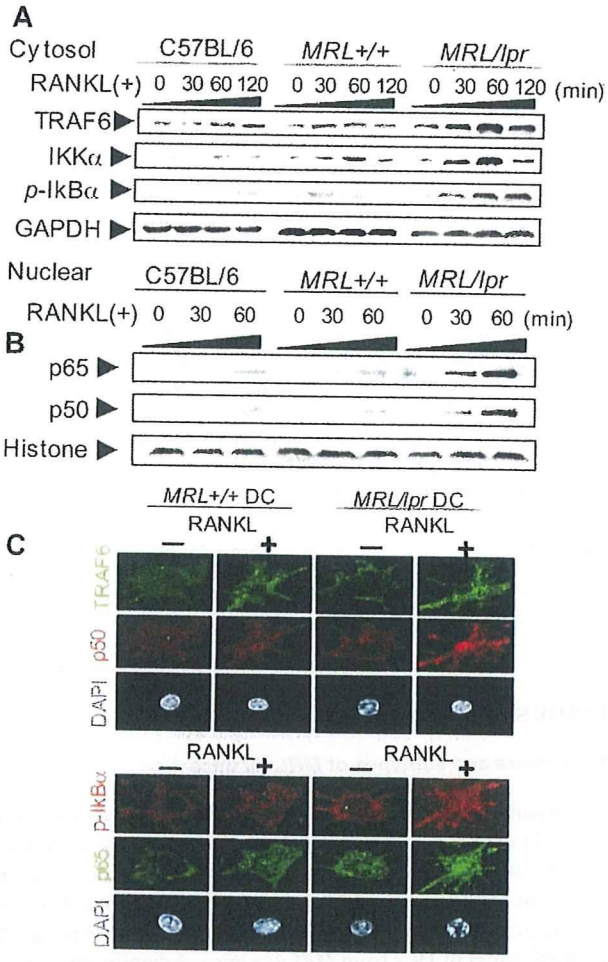

Figure 3. RANKL signaling molecules in *MRL/lpr* DCs. (A) The expressions of TRAF6, IKKα, and phospho-IκB (pIκB) of RANKL-stimulated BMDCs from C57BL/6, *MRL*$^{+/+}$, and *MRL/lpr* mice were detected using the cytoplasmic extracts by Western blot analysis. The BMDCs were stimulated with RANKL (100 ng/mL) from 0 to 120 minutes. GAPDH was used as a housekeeping protein. (B) Nuclear translocation of NF-κB (p65 and p50) of RANKL-stimulated BMDCs from C57BL/6, *MRL*$^{+/+}$, and *MRL/lpr* mice was detected by immunoblot. Histone was used as a housekeeping protein of the nuclear extracts. (C) Increased TRAF6 and p-IκB in the cytoplasm, and accelerated nuclear translocation of p50 and p65 in the nucleus of RANKL-stimulated *MRL/lpr* DCs were detected by confocal microscopic analysis. BMDCs from *MRL/lpr* and *MRL*$^{+/+}$ mice were stimulated for 48 hours with or without RANKL, fixed in 3% PFA on a glass slide, and stained with anti-p65, anti-p50, TRAF6, and p-IκBα followed by Alexa Fluor 488–labeled (green) or Alexa Fluor 568–labeled (red) anti-mouse or anti-rabbit IgG as the second antibodies. The nuclei were stained with DAPI. Original magnification, × 630. All data are representative of 3 to 5 independent experiments.

MRL/lpr DCs were observed in contrast to those from control DCs (Figure 3C). These findings suggest that the Fas molecule might regulate NF-κB activation of DCs through RANKL signaling.

Survival signaling of *MRL/lpr* DCs

To determine the growth of RANKL-stimulated BMDCs from *MRL/lpr* mice, the cell growth was analyzed by MTT assay. At 48 and 72 hours after RANKL stimulation, significantly increased growth of *MRL/lpr* DCs was observed compared with those of B6 and $MRL^{+/+}$ DCs (Figure 4A).

We next analyzed survival signaling molecules, Bcl-xL and Bcl-2, that are antiapoptotic molecules among the Bcl-2 family by flow cytometry. Enhanced expressions of both intracellular Bcl-xL and Bcl-2 in RANKL-stimulated *MRL/lpr* DCs were observed at 24 and 72 hours after the stimulation in contrast to that in $MRL^{+/+}$ DCs (Figure 4B). Moreover, prominent amounts of both Bcl-xL and Bcl-2 in RANKL-stimulated *MRL/lpr* DCs were detected compared with those in $MRL^{+/+}$ DCs using Western blot analysis (Figure 4C). By contrast, the expressions of Bax and Bid, apoptosis signaling molecules, in RANKL-stimulated *MRL/lpr* DCs were lower than those of $MRL^{+/+}$ DCs (Figure 4C). These data suggest that RANKL signal leads to enhancing the survival of Fas-deficient DCs through up-regulation of antiapoptotic molecules.

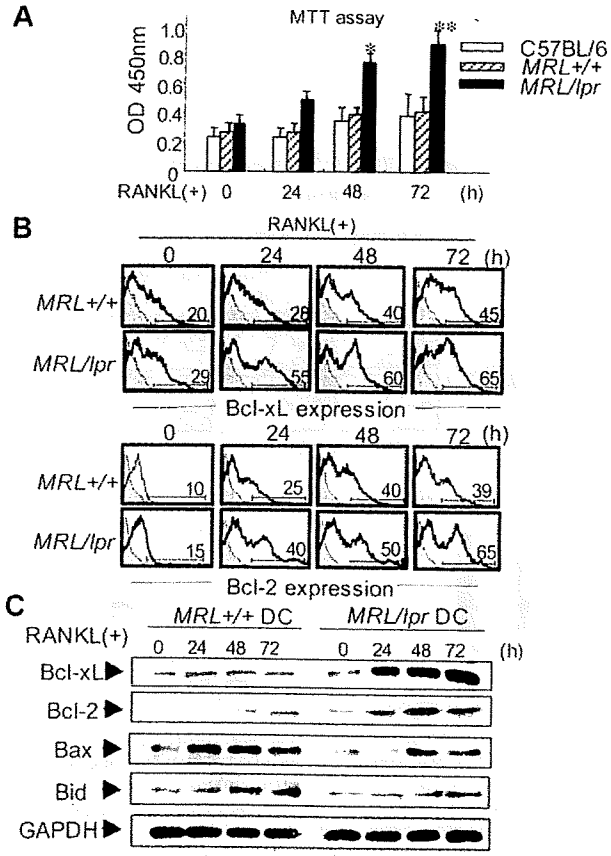

Figure 4. Antiapoptotic signaling through RANKL in *MRL/lpr* DCs. (A) BMDCs were stimulated with 100 ng/mL mouse recombinant RANKL from 0 to 72 hours, and the cell growth was analyzed by MTT assay. Data are means ± SD of triplicate samples and are representative of 4 independent experiments. $^{*}P > .05$; $^{**}P > .01$, *MRL/lpr* versus control mice. (B) BMDCs from *MRL/lpr* and control mice were stimulated with RANKL (100 ng/mL) from 0 to 72 hours, and the intracellular expressions of Bcl-xL and Bcl-2 were analyzed by flow cytometry. Numbers above horizontal lines indicate percent $Bcl\text{-}xL^{+}$ or $Bcl\text{-}2^{+}$ cells. Results are representative of 3 independent experiments. (C) BMDCs from $MRL^{+/+}$ and *MRL/lpr* mice were treated with RANKL (100 ng/mL) from 0 to 72 hours. Bcl-xL, Bcl-2, Bax, and Bid proteins were detected by Western blot analysis. GAPDH was used as a control for loading. Data are representative of 3 independent experiments.

RANKL signaling and Fas-mediated apoptosis of DCs

To examine the association of RANKL signaling with Fas-mediated apoptosis in DCs, Fas expression on BMDCs stimulated with RANKL was analyzed. A time-dependent increase in Fas expression on RANKL-stimulated BMDCs from normal B6 and $MRL^{+/+}$ mice, but not *MRL/lpr* mice, was observed (Figure 5A). We found an enhanced apoptosis of DCs when stimulated with both anti-Fas mAb and RANKL, whereas the apoptosis induced by RANKL or anti-Fas mAb was slightly increased (Figure 5B-C). Moreover, to clarify the molecular pathway of enhanced Fas-mediated apoptosis of DCs by RANKL, the movement of caspases downstream from Fas to undergo apoptosis was analyzed using $MRL^{+/+}$ DCs by Western blotting. Although a small amount of cleaved caspase-3 and caspase-9 of RANKL-stimulated $MRL^{+/+}$ DCs was observed, we detected an increased active form of caspase-3 and caspase-9 in the $MRL^{+/+}$ DCs stimulated with both anti-Fas and RANKL (Figure 5D). The activation of these caspases was clearly inhibited by the addition of caspase inhibitor (z-VAD; Figure 5D). Furthermore, the expression of $FLIP_L$, an inhibitory molecule against Fas-mediated apoptosis,[29,30] was significantly decreased by both RANKL and anti-Fas mAb parallel with the movement of the caspases (Figure 5D). It has been reported that $FLIP_L$ is constitutively expressed in DCs to play an inhibitory role for Fas-mediated apoptosis of DCs.[12,13,31] In addition, the expression of pro–caspase-8 was decreased by the stimulation of RANKL or anti-Fas mAb, and the expression was even lower with stimulation by both RANKL and anti-Fas mAb (Figure 5D). For *MRL/lpr* DCs, the expression of $FLIP_L$ was not reduced with RANKL stimulation (Figure 5E). These results strongly suggest that RANKL signaling may contribute to Fas-mediated apoptosis of DCs by controlling the expression of $FLIP_L$.

Effects of Fas siRNA on the function of DCs

To further confirm the enhanced antiapoptotic signal of RANKL-stimulated DCs by Fas deficiency in the *MRL/lpr* mice, we used siRNA of Fas to evaluate the apoptotic signaling and activation of normal BMDCs from control mice.

When BMDCs transfected with the siRNA of Fas were stimulated with RANKL for 48 hours, RANKL-induced Fas expression was decreased to the unstimulated level (Figure 6A). We next examined the inhibitory effect of Fas siRNA on RANKL/Fas-induced apoptosis of BMDCs. As expected, apoptosis of RANKL- and anti-Fas mAb-stimulated BMDCs was clearly inhibited by Fas siRNA, but not GAPDH siRNA or an irrelevant control (Figure 6B). Moreover, to clarify apoptosis signal of RANKL/Fas-mediated apoptosis of DCs, cleavage of caspase-3 was examined using Fas siRNA. A cleaved caspase-3 of BMDCs transfected with control siRNA was detected at 48 and 72 hours after RANKL stimulation, but no active form of caspase-3 of BMDCs transfected with Fas siRNA was observed (Figure 6C).

In addition, to confirm the role of Fas signal for the RANKL-induced activation of DCs, MHC class II expression, as 1 of some activation markers on RANKL-stimulated BMDCs treated with the siRNA, was analyzed by flow cytometry. RANKL-induced expression of MHC class II was still more enhanced by the transfection with Fas siRNA, but not control siRNA (Figure 6D). IL-12 secretion from RANKL-stimulated BMDCs of $MRL^{+/+}$ mice was

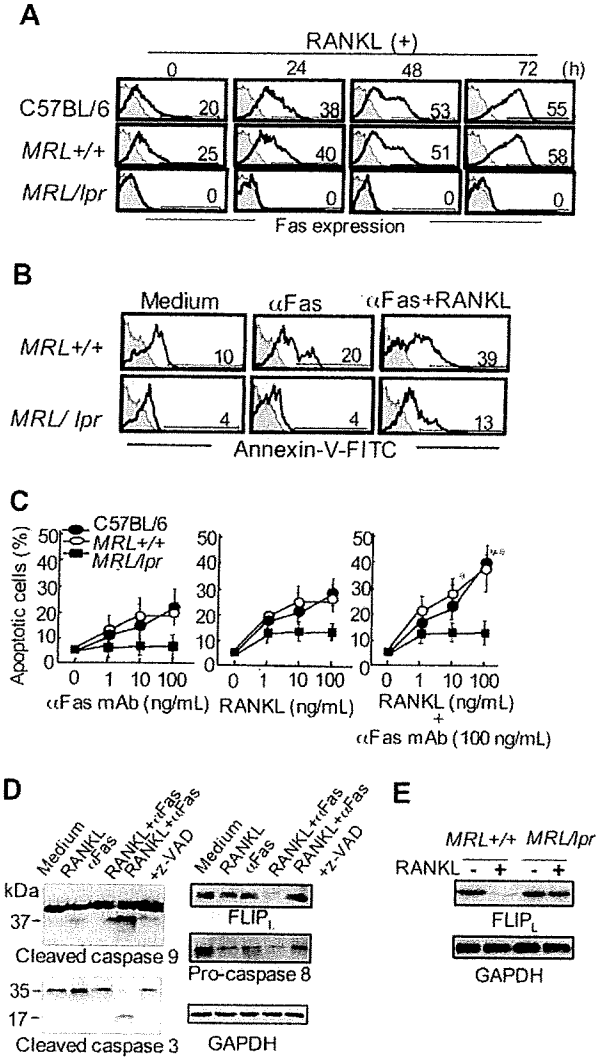

Figure 5. Fas signaling through RANKL in DCs. (A) BMDCs from normal B6, *MRL*$^{+/+}$, and *MRL/lpr* mice were cultured with RANKL from 0 to 72 hours. Fas expression on the DCs was detected by flow cytometry. Numbers above horizontal lines indicate percentage of Fas$^+$ cells. Results are representative of 3 independent experiments. (B) BMDCs from *MRL*$^{+/+}$ and *MRL/lpr* mice were incubated with anti-Fas mAb, or anti-Fas mAb and RANKL, for 48 hours. Apoptotic cells were detected by flow cytometric analysis. Numbers above horizontal lines indicate percentage of Annexin-V$^+$ cells. Results are representative of 3 independent experiments. (C) Apoptotic cells stimulated with anti-Fas mAb (1-100 ng/mL), RANKL (1-100 ng/mL), or RANKL and anti-Fas mAb (100 ng/mL) for 48 hours. B6 (●), *MRL*$^{+/+}$ (○), and *MRL/lpr* (■) mice are shown. Data are means ± SD of 3 independent experiments. $^*P > .05$; $^{**}P > .01$. (D) BMDCs (5×10^4 cells) were cultured treated with RANKL (100 ng/mL) and anti-Fas mAb (100 ng/mL) in the presence or absence of inhibitor z-VAD for 48 hours. The expressions of caspase-9, caspase-3, caspase-8, and FLIP$_L$ of the stimulated BMDCs from control mice were analyzed by Western blot. GAPDH was used as a control for loading. Results are representative of 3 independent experiments. (E) FLIP$_L$ expression of RANKL-stimulated BMDCs from *MRL*$^{+/+}$ and *MRL/lpr* mice was detected by immunoblot. GAPDH was used as a control for loading. Results are representative of 3 independent experiments.

elevated by the treatment with Fas siRNA, indicating that Fas deficiency positively controls RANKL signaling as observed in the DCs from *MRL/lpr* mice (Figure 6E). Moreover, the accelerated nuclear translocation of NF-κB in *MRL/lpr* DCs was observed in RANKL-stimulated BMDCs treated with Fas siRNA (Figure 6F). These findings indicate that RANKL-stimulated DCs from normal mice may be maintained by Fas-mediated apoptosis through caspase and NF-κB cascade.

Inhibitory effect of RANK siRNA on Fas-mediated apoptosis of DCs

To clarify the direct association between RANK/RANKL and Fas signaling of DCs, Fas-mediated apoptosis of RANK-deficient DCs was analyzed using the siRNA of RANK as shown in the protocol (Figure S1A, available on the *Blood* website; see the Supplemental Figures link at the top of the online article). The knockdown of RANK by the siRNA in BMDCs was confirmed by analyzing the protein expression of RANK on flow cytometry and Western blotting as shown in Figure S1B-C. Then, Fas expression and

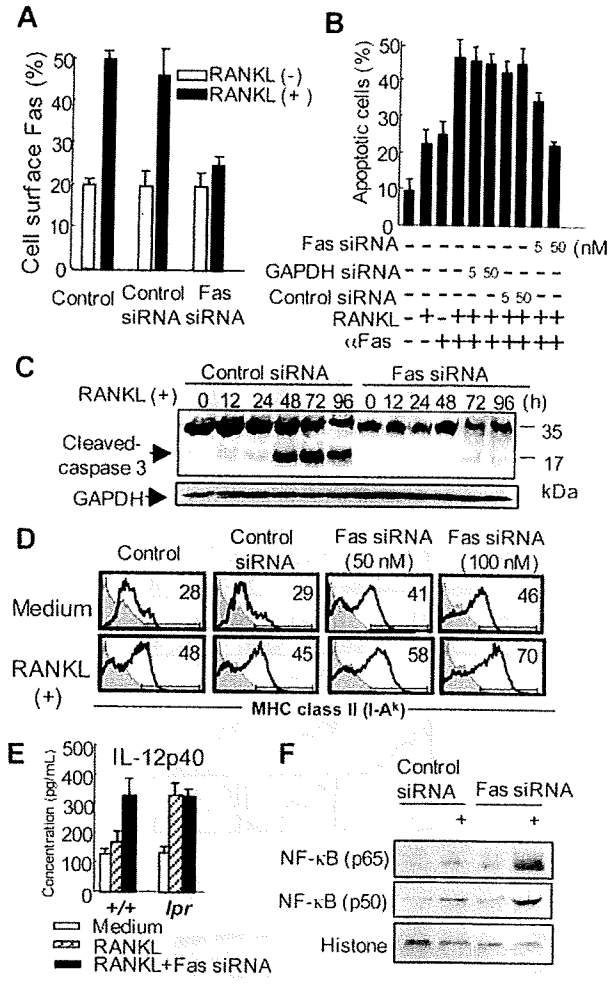

Figure 6. Effects of Fas siRNA on the functions of DCs. (A) Fas expression on Fas siRNA-transfected BMDCs from control mice was analyzed after the stimulation of RANKL. GAPDH siRNA or irrelevant oligonucleotides was used as control. Data are means ± SD of triplicate samples and are representative of 3 independent experiments. (B) Inhibitory effect of Fas siRNA on Fas and RANKL-induced apoptosis of BMDCs from control mice was observed. Apoptotic cells were detected by flow cytometric analysis. Data are means ± SD and representative of 3 independent experiments. (C) Fas siRNA-transfected BMDCs were stimulated with RANKL from 0 to 96 hours. Caspase-3 expression was analyzed by immunoblot. GAPDH was used as a control for loading. Data are representative of 3 independent experiments. (D) MHC class II expression on the Fas siRNA-transfected BMDCs stimulated with RANKL was detected by flow cytometric analysis. Numbers above horizontal lines indicate percentage of MHC class II$^+$ cells. Data are representative of 3 independent experiments. (E) Fas siRNA-transfected BMDCs from *MRL*$^{+/+}$ and *MRL/lpr* mice were stimulated with RANKL, and the secretion of IL-12 from the DCs was detected by ELISA. Data are means ± SD of triplicate samples and are representative of 3 independent experiments. (F) Nuclear translocation of NF-κB subunits (p65 and p50) was detected using the nuclear extracts of Fas siRNA-transfected BMDCs from control mice by Western blot analysis. Histone was used as a control for loading. Data are representative of 3 independent experiments.

apoptosis of RANK-deficient DCs from *MRL*$^{+/+}$ and *MRL/lpr* mice was analyzed as shown in Figure S1D-E. Expectedly, RANKL-induced Fas expression was decreased to the level of unstimulation in RANK-decifient DCs from *MRL*$^{+/+}$ mice (Figure S1D). Furthermore, the Fas- and RANKL-induced apoptosis was reduced to the level of anti-Fas stimulation (Figure S1E).

Influence of activated *MRL/lpr* DCs on arthritis

It is still unclear whether the activated and increased DCs from *MRL/lpr* mice influence autoimmune lesions such as arthritis in the mice. To determine whether the activated DCs from *MRL/lpr* mice may influence autoimmune lesions in vivo, the adoptive transfer of BMDCs stimulated with RANKL and CII into *MRL/lpr* mice at 4 weeks was performed to analyze arthritis lesions of the recipient mice. The histologic score of arthritis in the mice transferred with RANKL- and CII-stimulated *MRL/lpr* DCs was significantly higher at 12 and 16 weeks of age than those of the mice transferred with nonstimulated *MRL/lpr* DCs, RANKL- and CII-stimulated *MRL*$^{+/+}$ DCs, or the untreated mice (Figure 7A). Histologic findings of the recipient mice transferred with RANKL- and CII-stimulated *MRL/lpr* DCs showed severe subsynovial inflammation, synovial hyperplasia, pannus formation, cartilage erosion, and bone destruction (Figure 7B). In contrast, the histology of the mice transferred with RANKL- and CII-stimulated *MRL*$^{+/+}$ DCs was mild, similar to untreated *MRL/lpr* mice (Figure 7B). Anti-CII Ab and RF of sera from the recipient mice transferred with RANKL- and CII-stimulated *MRL/lpr* DCs were significantly increased (Figure 7C). Moreover, increased secretions of IFN-γ and IL-2, not IL-4 from T cells stimulated with anti-CD3 mAb of the recipient transferred with RANKL- and CII-stimulated *MRL/lpr* DCs, were detected compared with those of the control recipients (Figure 7D). These results indicate that the RANKL-stimulated DCs might play an important role in the acceleration of autoimmune arthritis in *MRL/lpr* mice through T helper 1 (Th1) response.

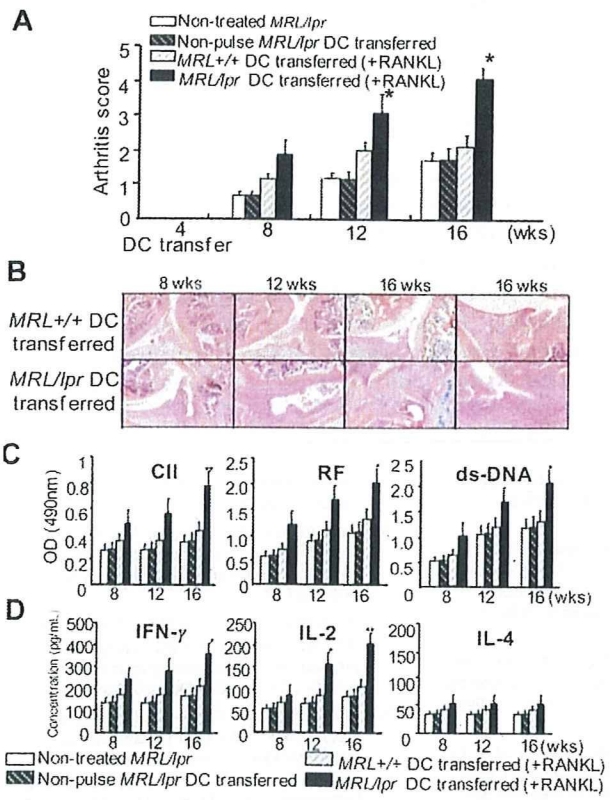

Figure 7. Effects of the RANKL-stimulated *MRL/lpr* DCs transfer on autoimmune arthritis. BMDCs pulsed with CII and stimulated with RANKL were transferred into *MRL/lpr* recipients (4 weeks of age). The recipient *MRL/lpr* mice were analyzed at 8 to 16 weeks of age. (A) Histologic score of autoimmune arthritis in *MRL/lpr* mice transferred with RANKL-stimulated *MRL/lpr* DCs was evaluated compared with control mice until 16 weeks of age. Data are means ± SD of 5 to 7 mice in each group. *$P > .05$; **$P > .01$, *MRL*$^{+/+}$ DCs versus *MRL/lpr* DCs transferred. (B) Histologic analysis of autoimmune lesions from *MRL/lpr* mice transferred with RANKL-stimulated *MRL/lpr* DCs and *MRL*$^{+/+}$ DCs at 8, 12, and 16 weeks of age was performed. The sections of joints from the recipients were stained with HE. Data are representative of 5 to 7 mice in each group. (C) RF, anti-CII antibodies, and anti-dsDNA antibodies of sera from the recipients at 16 weeks of age were detected by ELISA. (D) The secretions of IFN-γ, IL-2, and IL-4 in the supernatants from ILN T cells stimulated with anti-CD3 mAb were detected by ELISA. Data are means ± SD of triplicate samples and are representative of 5 to 7 mice in each group. *$P > .05$; **$P > .01$, *MRL*$^{+/+}$ DCs versus *MRL/lpr* DCs transferred.

Discussion

Studies in the past several years have established an important role of DCs in controlling many immune responses.[1,2] However, the mechanism of maintenance of peripheral DCs has been unclear. The present study indicates that the maintenance of DCs, including cell growth, activation, and apoptosis in the periphery, is regulated by a crosstalk between RANKL and Fas signaling, and that the RANKL/Fas system in DCs may play a key role for the maintenance of peripheral tolerance.

DCs are heterogeneous in terms of phenotype, localization, and function. Several DC subsets have been described based on surface expressions, such as CD11c, B220, CD11b, CD4, and CD8α.[3,4] It has been reported that plasmacytoid DCs induce Th2 cell differentiation in response to certain stimuli, and that myeloid DCs favor a Th1 response.[6] Among myeloid DCs, 4 subsets are known: CD11b$^+$CD8α^+, CD11b$^+$CD4$^+$, CD11b$^+$CD4$^-$, and CD11b^{low}CD8α^-CD4$^-$.[3,5,6] The function of each subset has been obscure. In this study, increased CD11c$^+$CD11b$^+$CD8α^+ myeloid DCs from *MRL/lpr* mice were observed, implying that the maintenance of Th1 DCs in the periphery may occur through Fas signaling, and that Th1 DCs from *MRL/lpr* mice might influence immune disorders such as autoimmune lesions and lymphadenopathy in the mice. It has been described that defective T-cell function of *MRL/lpr* mice plays a key role for pathogenesis of the immune disorder.[10,32,33] Our data demonstrate that dysfunction of DCs from *MRL/lpr* mice accelerates autoimmunity mediated by T and B cells.

It has been reported that the Fas-mediated apoptosis of DCs is resistant due to a constitutive FLIP that can block Fas-induced apoptosis, whereas Fas is expressed on the surface of DCs.[13,31] Upon Fas activation, a set of effector molecules is recruited to the receptor leading to form a signaling complex. Initially, FADD binds to Fas, recruits caspases, and activates a cascade of apoptosis. The present study indicates that Fas-mediated apoptosis of DCs can be induced by the addition of activated RANK/RANKL signaling, suggesting that there may be a crosstalk between the Fas and RANK pathway for DC maintenance in the periphery. In addition, our results indicate that the expression of FLIP$_L$ of DCs is controlled by RANKL and Fas signaling, leading to NF-κB activation. This is consistent with the recent report that cFLIP controls NF-κB activation and maintenance in lymphocytes and DCs.[34] The molecular mechanism may be mediated by activation-induced cell death (AICD), which is well known to act as a system to maintain the peripheral T cells through Fas-mediated apoptosis.[35-37] Activated or autoreactive T cells are considered to delete by

using AICD. Our data suggest that "AICD" of DCs may be mediated by the Fas and RANK pathway.

Bcl-2 family proteins, including Bcl-2 and Bcl-xL, are considered to be critical for DC survival, and to be regulated by NF-κB.[7,38] In this study, Bcl-xL and Bcl-2 expressions of *MRL/lpr* DCs were considerably up-regulated by RANKL stimulation, leading to hyperproliferation of DCs. In addition, NF-κB activation of *MRL/lpr* DCs induced by RANKL was accelerated, suggesting that the Fas signaling pathway might influence NF-κB activation via RANKL signaling in DCs. The NF-κB family has emerged as a key transducer of inflammatory signals to DC maturation and activation, and is well known to be activated by various stimuli such as RANK/RANKL, CD40, and toll-like receptors (TLRs).[14,39,40] Accelerated signaling pathways, including IKKα, IκB, and NF-κB downstream from TRAF6, was observed in *MRL/lpr* DCs stimulated by RANKL. Therefore, RANKL signaling leading to NF-κB activation through TRAF6 in DCs may be regulated by Fas-induced signaling.

DCs are crucial for the pathogenesis of autoimmune disease because of their potent antigen-presenting activity and unique ability to activate naive T cells.[41] DCs have also been described to prime autoreactive T cells and induce the local inflammation of the synovial membrane in arthritis.[42] It was reported that the transfer of collagen-pulsed BMDCs into congenic DBA/1 mice results in inflammatory arthritis.[43] In addition, antigen-pulsed DCs have been shown to induce disease in experimental autoimmune encephalomyelitis, a murine model of multiple sclerosis.[44] Our study showed that transfer of RANKL-stimulated *MRL/lpr* DCs pulsed with collagen into *MRL/lpr* mice clearly accelerates arthritis in the recipients, suggesting that the activated DCs stimulated by RANKL may accelerate autoreactivity of T and B cells to enhance the productions of pathogenic cytokines and autoantibidies in *MRL/lpr* mice. As for autoimmune arthritis of *MRL/lpr* mice, the increased DCs, especially myeloid DCs in the periphery, may play the key role for the pathogenesis. It was previously reported that an imbalance favoring development of DCs from myeloid-committed progenitors predisposes to autoimmune lesion in nonobese diabetic (NOD) mice.[45] Therefore, analyzing the differentiation and function of myeloid DCs may lead to understanding the pathogenic mechanism of autoimmune disease.

Taken together, the new finding in the present study is that the maintenance of DCs, including cell growth, activation, and apoptosis in the periphery, is regulated by crosstalk between RANKL and Fas signaling, and that the RANKL/Fas signaling in DCs may play a crucial role in the maintenance of immune tolerance.

Acknowledgments

The authors thank Ai Nagaoka, Hiroyo Amo, and Satoko Yoshida for technical assistance.

This work was supported by the Ministry of Education, Science, and Culture of Japan (Grants-in-Aid for Scientific Research nos. 17109016 and 17689049).

Authorship

Contribution: T.I. performed all experiments and wrote the manuscript; N.I. codesigned experiments, coperformed confocal microscopic analysis, and wrote the manuscript; K.M. codesigned experiments and wrote the manuscript; M.K. coperformed ELISA with T.I.; R.A. performed Western blot analysis; Y.H. unified the project and wrote the manuscript.

Conflict-of-interest disclosure: The authors declare no competing financial interests.

Correspondence: Yoshio Hayashi, Department of Oral Molecular Pathology, Institute of Health Biosciences, The University of Tokushima Graduate School, 3–18-15 Kuramotocho, Tokushima 770-8504, Japan; e-mail: hayashi@dent.tokushima-u.ac.jp.

References

1. Banchereau J, Steinman RM. Dendritic cells and the control of immunity. Nature. 1998;392:245-252.
2. Banchereau J, Briere F, Caux C, et al. Immunobiology of dendritic cells. Annu Rev Immunol. 2000; 18:767-811.
3. Shortman K, Liu YJ. Mouse and human dendritic cell subtypes. Nat Rev Immunol. 2002;2:151-161.
4. Salomon B, Cohen JL, Masurier C, Klatzmann D. Three populations of mouse lymph node dendritic cells with different origins and dynamics. J Immunol. 1998;160:708-717.
5. Vremec D, Shortman K. Dendritic cell subtypes in mouse lymphoid organs: cross-correlation of surface markers, changes with incubation, and differences among thymus, spleen, and lymph nodes. J Immunol. 1997;159:565-573.
6. Nakano H, Yanagita M, Gunn MD. CD11c(+)B220(+) Gr-1(+) cells in mouse lymph nodes and spleen display characteristics of plasmacytoid dendritic cells. J Exp Med. 2001;194:1171-1178.
7. Hou WS, Van Parijs L. A Bcl-2-dependent molecular timer regulates the lifespan and immunogenicity of dendritic cells. Nat Immunol. 2004;5: 583-589.
8. Matsue H, Edelbaum D, Hartmann AC, et al. Dendritic cells undergo rapid apoptosis in vitro during antigen-specific interaction with CD4+ T cells. J Immunol. 1999;162:5287-5298.
9. Nagata S, Golstein P. The Fas death factor. Science. 1995;267:1449-1456.
10. Chen M, Wang YH, Wang Y, et al. Dendritic cell apoptosis in the maintenance of immune tolerance. Science. 2006;311:1160-1164.
11. Fields ML, Sokol CL, Eaton-Bassiri A, Seo S, Madaio MP, Erikson J. Fas/Fas ligand deficiency results in altered localization of anti-double-stranded DNA B cells and dendritic cells. J Immunol. 2001;167:2370-2378.
12. Ashany D, Savir A, Bhardwaj N, Elkon KB. Dendritic cells are resistant to apoptosis through the Fas (CD95/APO-1) pathway. J Immunol. 1999; 163:5303-5311.
13. Willems F, Amraoui Z, Vanderheyde N, et al. Expression of c-FLIP(L) and resistance to CD95-mediated apoptosis of monocyte-derived dendritic cells: inhibition by bisindolylmaleimide. Blood. 2000;95:3478-3482.
14. Wong BR, Rho J, Arron J, et al. TRANCE is a novel ligand of the tumor necrosis factor receptor family that activates c-Jun N-terminal kinase in T cells. J Biol Chem. 1997;272:25190-25194.
15. Anderson DM, Maraskovsky E, Billingsley WL, et al. A homologue of the TNF receptor and its ligand enhance T-cell growth and dendritic-cell function. Nature. 1997;390:175-179.
16. Simonet WS, Lacey DL, Dunstan CR, et al. Osteoprotegerin: a novel secreted protein involved in the regulation of bone density. Cell. 1997;89: 309-319.
17. Kong YY, Yoshida H, Sarosi I, et al. OPGL is a key regulator of osteoclastogenesis, lymphocyte development and lymph-node organogenesis. Nature. 1999;397:315-323.
18. Fata JE, Kong YY, Li J, et al. The osteoclast differentiation factor osteoprotegerin-ligand is essential for mammary gland development. Cell. 2000;103:41-50.
19. Wu X, Pan G, McKenna MA, Zayzafoon M, Xiong WC, McDonald JM. RANKL regulates Fas expression and Fas-mediated apoptosis in osteoclasts. J Bone Miner Res. 2005;20:107-116.
20. Wong BR, Josien R, Lee SY, et al. TRANCE (tumor necrosis factor [TNF]-related activation-induced cytokine), a new TNF family member predominantly expressed in T cells, is a dendritic cell-specific survival factor. J Exp Med. 1997;186: 2075-2080.
21. Inaba K, Inaba M, Romani N, et al. Generation of large numbers of dendritic cells from mouse bone marrow cultures supplemented with granulocyte/macrophage colony-stimulating factor. J Exp Med. 1992;176:1693-1702.
22. Lutz MB, Kukutsch N, Ogilvie AL, et al. An advanced culture method for generating large quantities of highly pure dendritic cells from mouse bone marrow. J Immunol Methods. 1999;223:77-92.
23. Edwards CK III, Zhou T, Zhang J, et al. Inhibition of superantigen-induced proinflammatory cytokine production and inflammatory arthritis in MRL-lpr/lpr mice by a transcriptional inhibitor of TNF-alpha. J Immunol. 1996;157:1758-1772.

24. Darnay BG, Haridas V, Ni J, Moore PA, Aggarwal BB. Characterization of the intracellular domain of receptor activator of NF-kappaB (RANK): interaction with tumor necrosis factor receptor-associated factors and activation of NF-kappab and c-Jun N-terminal kinase. J Biol Chem. 1998;273: 20551-20555.
25. Wong BR, Besser D, Kim N, et al. TRANCE, a TNF family member, activates Akt/PKB through a signaling complex involving TRAF6 and c-Src. Mol Cell. 1999;4:1041-1049.
26. Ouaaz F, Arron J, Zheng Y, Choi Y, Beg AA. Dendritic cell development and survival require distinct NF-kappaB subunits. Immunity. 2002;16: 257-270.
27. Darnay BG, Ni J, Moore PA, Aggarwal BB. Activation of NF-kappaB by RANK requires tumor necrosis factor receptor-associated factor (TRAF) 6 and NF-kappaB-inducing kinase: identification of a novel TRAF6 interaction motif. J Biol Chem. 1999;274:7724-7731.
28. Baud V, Liu ZG, Bennett B, Suzuki N, Xia Y, Karin M. Signaling by proinflammatory cytokines: oligomerization of TRAF2 and TRAF6 is sufficient for JNK and IKK activation and target gene induction via an amino-terminal effector domain. Genes Dev. 1999;13:1297-1308.
29. Irmler M, Thome M, Hahne M, et al. Inhibition of death receptor signals by cellular FLIP. Nature. 1997;388:190-195.
30. Scaffidi C, Schmitz I, Krammer PH, Peter ME. The role of c-FLIP in modulation of CD95-induced apoptosis. J Biol Chem. 1997;388:1541-1548.
31. Rescigno M, Piguet V, Valzasina B, et al. Fas engagement induces the maturation of dendritic cells (DCs), the release of interleukin (IL)-1beta, and the production of interferon gamma in the absence of IL-12 during DC-T cell cognate interaction: a new role for Fas ligand in inflammatory responses. J Exp Med. 2000;95:1661-1668.
32. Rieux-Laucat F, Le Deist F, Hivroz C, et al. Mutations in Fas associated with human lymphoproliferative syndrome and autoimmunity. Science. 1995;268:1347-1349.
33. Fisher GH, Rosenberg FJ, Straus SE, et al. Dominant interfering Fas gene mutations impair apoptosis in a human autoimmune lymphoproliferative syndrome. Cell. 1995;81:935-946.
34. Golks A, Brenner D, Krammer PH, Lavrik IN. The c-FLIP-NH2 terminus (p22-FLIP) induces NF-kappaB activation. J Exp Med. 2006;203:1295-1305.
35. Chen Y, Inobe J, Marks R, Gonnella P, Kuchroo VK, Weiner HL. Peripheral deletion of antigen-reactive T cells in oral tolerance. Nature. 1995; 376:177-180.
36. Van Parijs L, Ibraghimov A, Abbas AK. The roles of costimulation and Fas in T cell apoptosis and peripheral tolerance. Immunity. 1996;4:321-328.
37. Ishimaru N, Yanagi K, Ogawa K, Suda T, Saito I, Hayashi Y. Possible role of organ-specific autoantigen for Fas ligand-mediated activation-induced cell death in murine Sjogren's syndrome. J Immunol. 2001;167:6031-6037.
38. Hon H, Rucker EB III, Hennighausen L, Jacob J. bcl-xL is critical for dendritic cell survival in vivo. J Immunol. 2004;173:4425-4432.
39. Park Y, Lee SW, Sung YC. Cutting edge: CpG DNA inhibits dendritic cell apoptosis by up-regulating cellular inhibitor of apoptosis proteins through the phosphatidylinositide-3′-OH kinase pathway. J Immunol. 2002;168:5-8.
40. Rescigno M, Martino M, Sutherland CL, Gold MR, Ricciardi-Castagnoli P. Dendritic cell survival and maturation are regulated by different signaling pathways. J Exp Med. 1998;188: 2175-2180.
41. Legge KL, Gregg RK, Maldonado-Lopez R, et al. On the role of dendritic cells in peripheral T cell tolerance and modulation of autoimmunity. J Exp Med. 2002;195:217-227.
42. Thomas R, Davis LS, Lipsky PE. Rheumatoid synovium is enriched in mature antigen-presenting dendritic cells. J Immunol. 1994;152:2613-2623.
43. Leung BP, Conacher M, Hunter D, McInnes IB, Liew FY, Brewer JM. A novel dendritic cell-induced model of erosive inflammatory arthritis: distinct roles for dendritic cells in T cell activation and induction of local inflammation. J Immunol. 2002;169:7071-7077.
44. Menges M, Rossner S, Voigtlander C, et al. Repetitive injections of dendritic cells matured with tumor necrosis factor alpha induce antigen-specific protection of mice from autoimmunity. J Exp Med. 2002;195:15-21.
45. Steptoe RJ, Ritchie JM, Harrison LC. Increased generation of dendritic cells from myeloid progenitors in autoimmune-prone nonobese diabetic mice. J Immunol. 2002;168:5032-5041.

特集I　T細胞レセプターからのシグナル伝達

T細胞レセプターシグナルとNF-κB*

石丸直澄**
岸本英博***
林　良夫**

Key Words：NF-κB, T cell receptor, IκB, activation, NF-κB2(p100/p52)

はじめに

T細胞の活性化や増殖にはT細胞そのものが産生するサイトカインや増殖因子が必須である．そのサイトカインや増殖因子の転写を制御している転写因子の中でもっとも重要な位置に存在しているのがnuclear factor(NF)-κBである．NF-κBは，IL-2をはじめとしたサイトカインおよびサイトカインレセプター，増殖因子，細胞接着分子，細胞周期に関連する遺伝子，アポトーシス関連遺伝子などT細胞の生死にかかわる重要な遺伝子の転写調節を司っている[1]．一般的にT細胞受容体(T cell receptor；TCR)，CD28を中心とした副刺激分子およびサイトカインレセプターなどを介した刺激からさまざまなシグナル分子を経由してNF-κBの内在性阻害因子であるIκBのリン酸化，ユビキチン化および断片化によってIκBから解離したNF-κB分子のヘテロおよびホモダイマーが細胞質から核内に移行し，標的遺伝子上に存在するκBサイトを介して転写が調節され，さまざまな重要因子が合成されT細胞の機能獲得に用いられている．最近，IκBによるNF-κBの制御機構に加えて新たにNF-κB2による調節機構が明らかにされ，自己免疫疾患の病態発症におけるNF-κBシグナルの謎が解き明かされようとしている．

2つのNF-κB経路

転写因子であるNF-κBは免疫細胞における多くの炎症反応を制御している．NF-κBにはN末にDNA結合に重要な共通のRelホモロジー領域を有するNF-κB1(p105-p50)，NF-κB2(p100-p52)，RelA(p65)，RelB, c-Relの5つのサブユニットがあり(図1)，それらのサブユニットがヘテロダイマーあるいはホモダイマーとなり核内移行し，細胞の活性化や増殖などに重要な遺伝子の転写調節を司ることが知られている[2]．NF-κB経路にはNF-κB1とRelAの複合体によって調節される古典的経路(classical NF-κB pathway)と，NF-κB2とRelBの複合体によって調節される非古典的経路(non-classical NF-κB pathway)が報告されている[3](図2)．

TCR/CD3関連シグナルとNF-κB

T細胞では主にTCRからの刺激がさまざまな伝達分子を介して古典的NF-κBの活性化につながることがよく知られている[4]．まず，TCRからの抗原刺激によりTCR/CD3分子複合体に連動してZAP70, Fyn, Vavやposphoinositide 3-kinase

* The critical NF-κB pathway through T cell receptor.

** Naozumi ISHIMARU, D.D.S., Ph.D. & Yoshio HAYASHI, D.D.S., Ph.D.: 徳島大学大学院ヘルスバイオサイエンス研究部口腔分子病態学分野〔〒770-8504 徳島市蔵本町3-18-15〕; Department of Oral Molecular Pathology, Institute of Health Biosciences, The University of Tokushima Graduate School, Tokushima 770-8504, JAPAN
*** Hidehiro KISHIMOTO, M.D., Ph.D.: 東京理科大学生命科学研究所免疫生物学研究部門

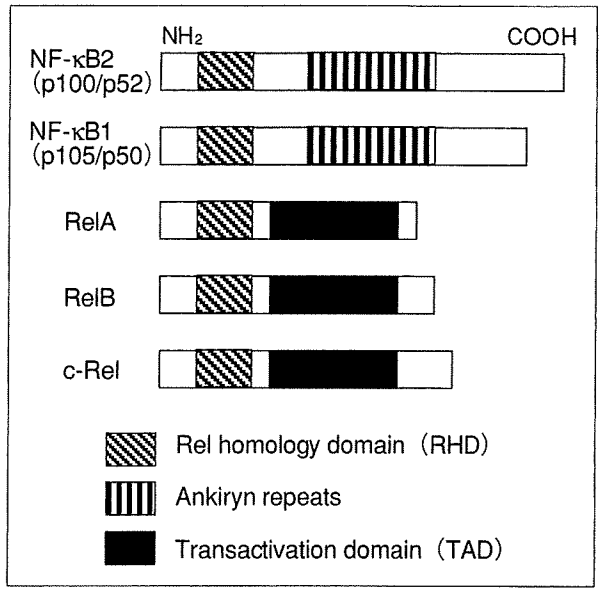

図1　NF-κBサブユニットの構造

(PI3K)といったアダプター分子を介して，protein kinase C θ(PKCθ)，caspase-recruitment domain-containing membrane-associated guanylate kinase protein 1(CARMA1)のリン酸化へと進んでいく．PKCθより上流のシグナルはAP-1, NFATといったNF-κBとは別のルートによるT細胞の活性化経路と共通しているが，3-phosphoinositide-dependent protein kinase 1(PDK1)から引き続いて誘導されるPKCθとCARMA1のリン酸化はNF-κBの活性化に重要な起点となっている．PKCθのリン酸化に続いてCARMA1, B-cell lymphoma 10 (Bcl-10)，mucosa-associated-lymphoid-tissue lymphoma-translocation gene 1(MALT-1)複合体を介してIκB kinase(IKK)の活性化につながっていく[5)6)]．また，PKCθが直接IKKに結合してIKKの活性を調節していることも明らかにされている[7)]．一方，副刺激分子であるCD28からのシグナルに関しては，TCRの刺激がない状態でCD28刺激を入れてもNF-κBの活性化は不十分であり，T細胞の活性化および増殖といった正常な機能獲得には至らない．CD28分子からのシグナルはTCRの下流のPI3KやAKTなどのアダプター分子を経由して上記のPKC/CARMA1/Bcl-10/MALT-1を介してIKKの活性化につながり，TCRからのNF-κBシグナルを量的に調節しているものと考えられる．IL-2レセプターなどのサイトカインレセプターからのシグナルに関してもTCRの下流のシグナル分子と合流していることが知られている[8)9)]．

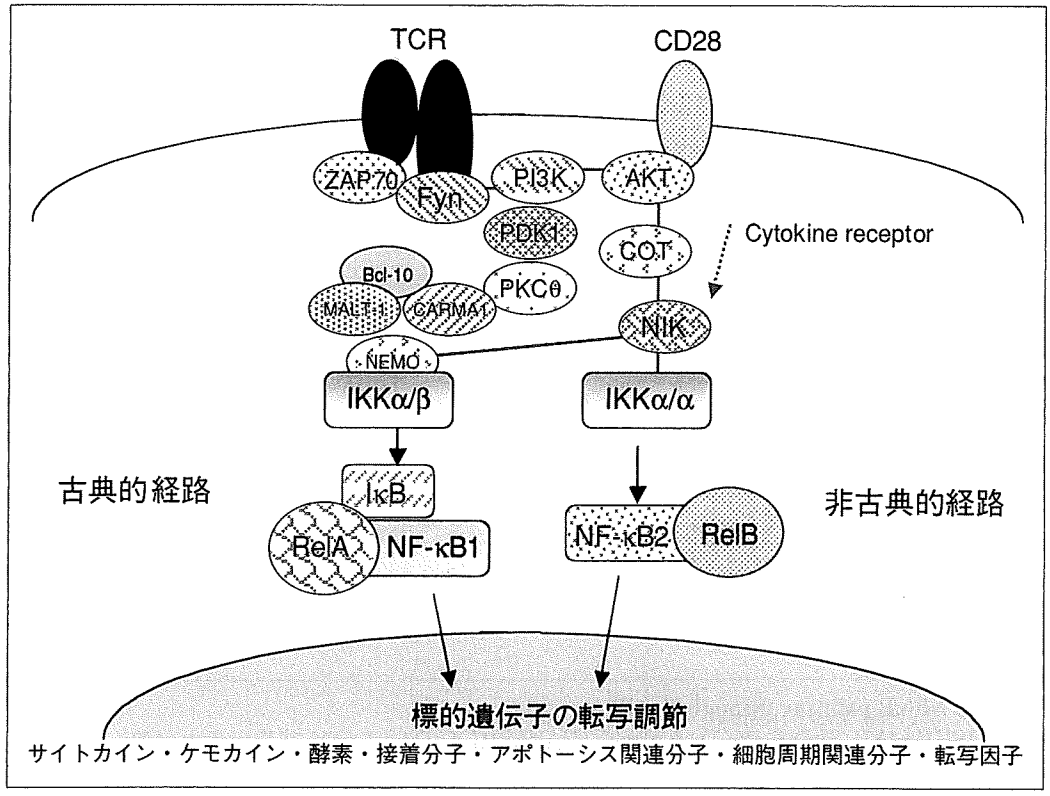

図2　T細胞レセプターと古典的NF-κB経路および非古典的(新規)NF-κB経路
T細胞あるいはCD28の下流におけるNF-κBの転写活性に至る過程の概略図を示す．

IκBによる制御システム

NF-κBの活性化の引き金となるのが，NF-κB分子と結合しているIκBのリン酸化から始まるユビキチン化，断片化である．通常はNF-κB分子は細胞質でIκBと結合することによって核内に移行しないように制御されている[5]．CARMA1/Bcl-10/MALT-1複合体の活性化からIKKのキナーゼ活性が高まりIκBのリン酸化が誘導されると，IκB分子はユビキチン化を受けた後プロテアソームにより分断化されることによりNF-κBの核内移行を阻害できなくなる．つまり，IκBによる制御が解除されるときにNF-κBの活性化は開始される．正常マウスのCD4陽性T細胞を抗TCR抗体および抗CD28抗体により刺激すると，IκBのリン酸化および断片化，さらに，NF-κB分子の核内移行が観察される(図3)．IκB分子をリン酸化するのがIKK複合体であり，2つのキナーゼと調節蛋白であるNF-κB essential molecule(NEMO)から構成されるIKKはCARMA1/Bcl-10/MALT-1を介してNEMOのユビキチン化，IKKαまたはIKKβのリン酸化を通したキナーゼ活性の上昇によりIκBのリン酸化に結びついていく[10]．シグナルを制御する分子を各ステップで解除していくことにより，NF-κBの活性化が開始される．逆に言えば，NF-κBはいくつもの制御システムにより精巧に調節されていると言ってよい．ひとたび，NF-κB分子が核内に移行するとT細胞の機能にきわめて重要な遺伝子の転写調節が進行するのである．

NF-κBの核内移行

NF-κB分子が核内移行すると標的遺伝子のプロモーター領域に存在するκB結合部位にNF-κB分子が直接結合することにより，その遺伝子の転写活性が開始される．5つのNF-κBサブユニットの中で実際に標的遺伝子の転写を司るのはC末に転写活性領域を有するRelA(p65)，RelB, c-Relである(図1)．一方，NF-κB1(p105/p50)とNF-κB2(p100/p52)には転写活性領域は存在しないが，核内移行に重要なシグナルモチーフを有していることから，NF-κB1およびNF-κB2は他の3つのサブユニットとのヘテロダイマーの形成により核内移行を最終的に調節していると考えられる[3]．NF-κBはT細胞の活性化や増殖に重要なIL-2およびその受容体の一つであるCD25などのようなサイトカインやサイトカイン受容体，ケ

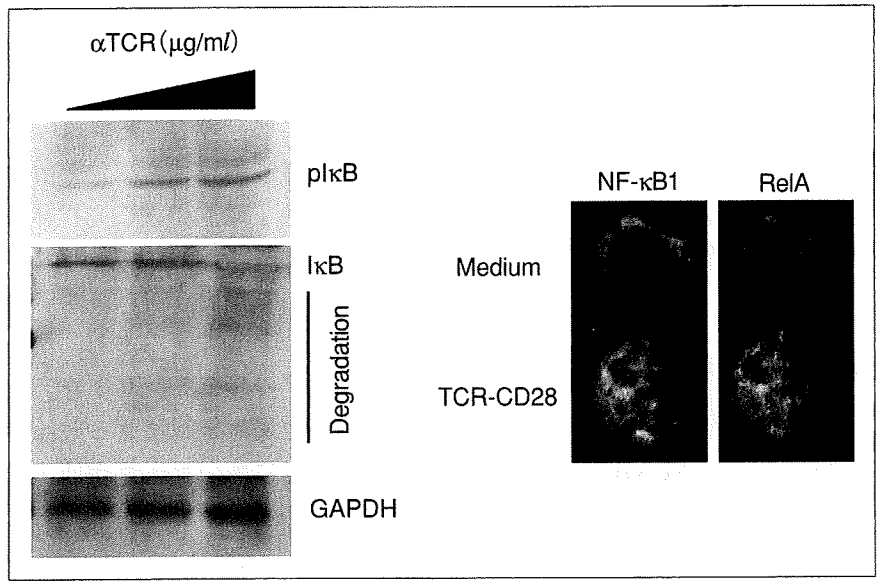

図3 NF-κBの活性化

左：正常マウス脾臓からのCD4陽性細胞に抗TCR抗体(0～1μg/ml)および抗CD28抗体(20μg/ml)で刺激し，抗リン酸化IκB抗体によりウエスタンブロットを行った．さらに，IκBの断片化を確認した．ローディングコントロールとしてglyceraldehyde phosphate dehydrogenase(GAPDH)を用いた．

右：刺激後のCD4陽性T細胞のNF-κB1およびRelAの核内移行をコンフォーカル顕微鏡解析により確認した．

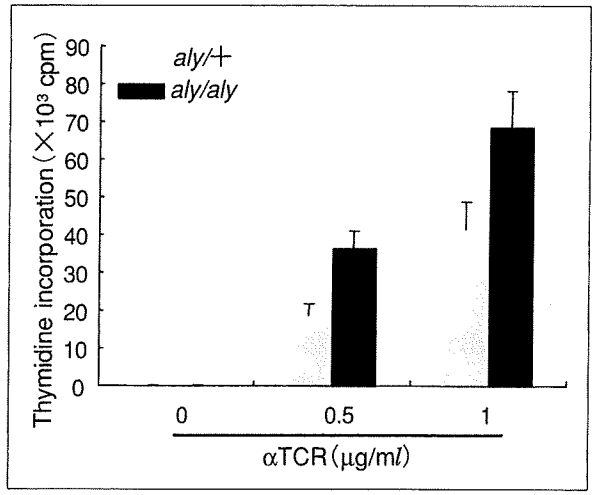

図4　NF-κB2不全マウスのナイーブT細胞の反応性
*aly/aly*マウスと対照マウスの脾臓CD4陽性細胞に抗TCR抗体(0～1 μg/m*l*)および抗CD28抗体(20μg/m*l*)で48時間刺激し，培養の最終12時間における[^{3}H]標識チミジンの取り込みをシンチレーションカウンターにより計測した．

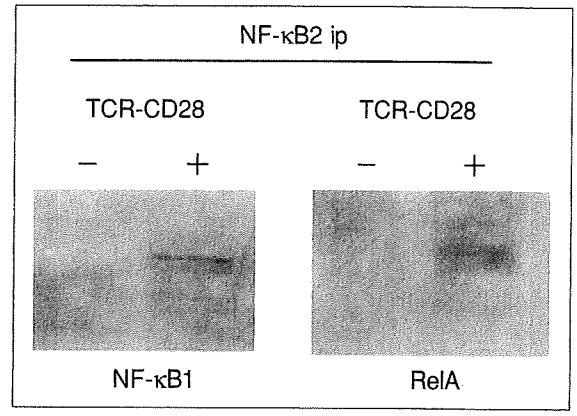

図5　NF-κB2分子とNF-κB1およびRelAとの結合
正常マウス脾臓からのCD4陽性細胞に抗TCR抗体(1 μg/m*l*)および抗CD28抗体(20μg/m*l*)で刺激し，細胞質分画蛋白質を抽出後，NF-κB2抗体で免疫沈降(ip)を行い，ウエスタンブロット法によりNF-κB1およびRelAを検出した．

モカイン，接着分子，アポトーシス関連因子，細胞周期関連因子などT細胞の分化，維持および機能獲得に重要な遺伝子群を標的としている[11]．さらに，NF-κB遺伝子自体をNF-κBが転写調節していることが知られており，転写因子自体の発現調節を自身で制御しているという点はNF-κBそのものの動態を知る上で重要である[12]．また，各サブユニットがどの標的遺伝子の転写調節に関連しているのかの区別は明確にできていない．各サブユニットの組み合わせや，シグナルカスケードの各中継ポイントにおけるシグナルの質的および量的な違いなど複雑な因子の影響によりNF-κBの活性システムが調節されていることが想定される．

T細胞における非古典的経路

では，T細胞の活性化に非古典的NF-κB経路は関与してないのであろうか．NF-κB2およびRelBの遺伝子欠損マウスでもT細胞に機能不全や自己免疫病変の発症が報告されている[13][14]．

正常マウスのCD4陽性T細胞への抗TCR抗体および抗CD28抗体による活性化におけるNF-κBの動態を観察すると，活性の初期段階ではNF-κB1/RelAのヘテロダイマーの核内移行が中心であり，非古典的経路であるNF-κB2/RelBの核内移行はほとんど認められず，増殖期を含む後期段階ではNF-κB2/RelBの核内移行が確認されるが[15]，その役割は不明であった．非古典的NF-κB経路ではTCRおよびCD28からのシグナル伝達に関しては古典的経路ほど明らかにされていない．PKCθ，PI3KおよびAKTからNF-κB-inducing kinase(NIK)を活性化し，NIKはIKKαをリン酸化することによりNF-κB2(p100)のIκB様配列をリン酸化，ユビキチン化する．古典的NF-κB経路と同様にプロテアソームにより断片化され，p52にプロセッシングされることによりp52/RelBヘテロダイマーが核内に移行することが知られている[3]．NIK遺伝子の点変異マウスである*aly/aly*マウスは末梢CD4陽性T細胞の抗CD3抗体による増殖反応が対照マウスに比較して低下していることが報告されているが[16]，CD4陽性T細胞の中で，メモリー型のT細胞を除去し，ナイーブ型のCD4陽性T細胞のみを抗TCRおよび抗CD28抗体で刺激して増殖反応を観察すると，対照マウスに比較して有意に高い反応性が認められた(図4)．一方で，*aly/aly*マウスのメモリー型のみの増殖反応はきわめて低くなっていることが判明した[15]．NIK欠損マウスにおいてもナイーブ型CD4陽性T細胞の増殖活性は有意に上昇していることを確認した．さらに，NF-κB2欠損マウスにおいてもT細胞の過剰増殖が報告されていることから，ナイーブCD4陽性T細胞の活性化における非古典的NF-κB経路(NF-κB2/RelB)の負の制御機構が存

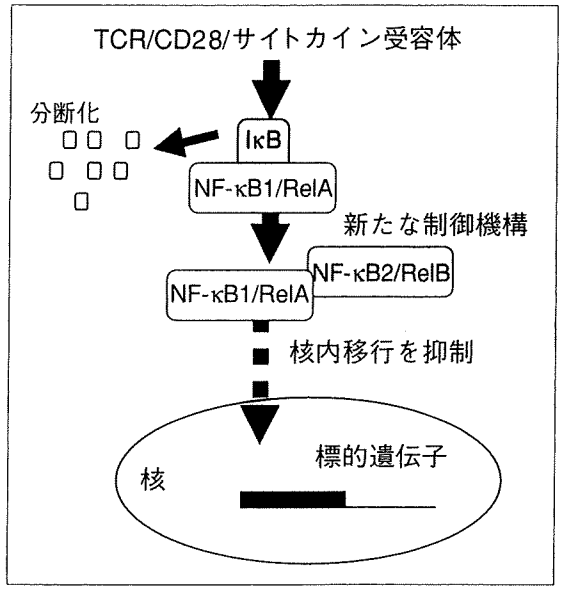

図6 NF-κB2による古典的NF-κB経路の新たな制御機構

在することが明らかになった．また，T細胞のナイーブからメモリー型に至る段階でNF-κBのサブユニットの役割が分担されている可能性が示された．

NF-κBサブユニット間のクロストーク

NF-κBのサブユニット間での結合に関しては，RelA, RelBおよびc-Relでのホモダイマー以外は5つのサブユニット間でヘテロダイマー，ホモダイマーを形成しうることが知られているが，それらのT細胞における生理的および機能的役割は明らかにされていなかった．上述のNF-κB2の制御機構の細胞内での機序を知るために，正常マウスからナイーブ型($CD44^{low}$)のCD4陽性T細胞を用いて抗TCRおよび抗CD28抗体で刺激した後に，細胞質分画の蛋白質を抽出し，NF-κB2抗体で免疫沈降して各NF-κBサブユニットに対する抗体でウエスタンブロット法により各サブユニットとNF-κB2の直接の結合を確認したところ，NF-κB1およびRelA蛋白が検出された(図5)．一方，*aly/aly*マウスではナイーブ型CD4陽性細胞に刺激を加えると，NF-κB2の合成が阻害されることも判明し，NF-κB2とNF-κB1およびRelAとの結合は観察されなかった[15]．この所見は*aly/aly*マウスのナイーブ型CD4陽性T細胞の過剰な反応性がNF-κB2分子を介した制御機構の異常により生じていることを示唆している．従来のIκBによるNF-κBの活性化制御機構に加え，NF-κB2分子がNF-κB1/RelA複合体と細胞質で直接結合することにより，その複合体の核内移行を阻害することでNF-κBの活性化シグナルを調節する新たな免疫制御機構が明らかにされた(図6)．一方で，メモリー型($CD44^{high}$)CD4陽性T細胞に関してはこの制御システムは働いていないことから，T細胞の活性化段階でNF-κBの各サブユニットの役割が異なっている可能性が示された．非古典的NF-κB経路と古典的NF-κB経路のクロストークはT細胞のみではなく，たとえば，破骨細胞の活性化過程においても報告されていることから，別の細胞種においても，このシステムがなんらかの機能調節に関与している可能性がある[12)17)]．

NF-κBと免疫疾患

これまでにNF-κB各サブユニットの遺伝子欠損マウスの解析からT細胞におけるNF-κBの生体内での役割が明らかにされている．たとえば，NF-κB1欠損マウスのT細胞では増殖の抑制およびTh_2タイプのサイトカインの産生減少が観察され，ヒト多発性硬化症の疾患モデル(EAE)での病態感受性の上昇および*Leishmania major*への易感染性がみられ，また，RelA欠損マウスは胎生致死であるが，胎児肝細胞キメラを用いた実験でT細胞の機能低下が報告されている[18)~22)]．一方，RelB欠損マウスは2～3か月齢で重度の自己免疫性貧血および全身の炎症で死亡し，T細胞の機能低下も観察されている[13)]．さらに，NF-κB2欠損マウスではT細胞の過反応がみられ，c-Rel欠損マウスではT細胞の反応性の低下やEAEに対する疾患感受性の低下が知られている[23)24)]．加えて，NF-κB2分子を調節する因子であるNIKの欠損マウスおよびNIK遺伝子の変異マウスにおいてT細胞の増殖は抑制され，多臓器に自己免疫病変が発症することが報告されている[25)]．しかし，T細胞の各活性化段階でのNF-κBの詳細な役割や各サブユニット同士の相互作用と自己免疫との関係は不明な点が多かった．

*aly/aly*マウスやNIK欠損マウスにおける自己免疫病変の発症には胸腺由来の$CD25^+CD4^+$調節性T細胞の数的な減少および質的な障害が自己免

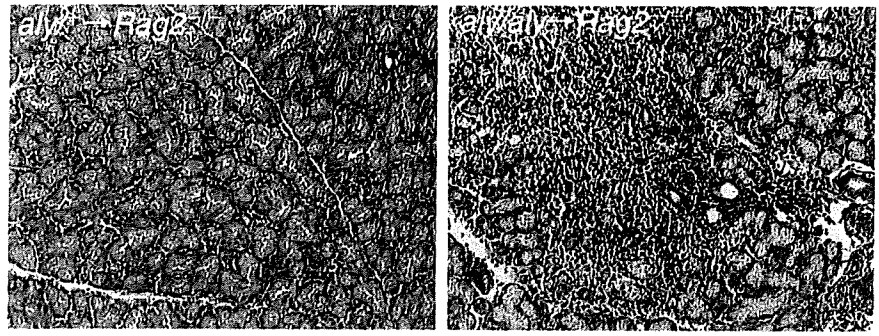

図7　NF-κB2機能不全と自己免疫
*aly/aly*マウスと対照マウスのナイーブ型CD4陽性T細胞を*Rag2*遺伝子欠損マウスに移入後6週における涙腺の病理組織像を示す．*aly/aly*→*Rag2*$^{-/-}$群では腺組織の破壊を伴ったリンパ球浸潤が認められる．

疫の発症に重要であることが報告されている[16)26)]．しかし，*aly/aly*マウスのナイーブ型CD25^{-}CD4^{+}T細胞を*Rag2*遺伝子欠損マウスに移入すると，本来の*aly/aly*マウスに発症する自己免疫病変よりもはるかに激しい自己免疫性病変が肺や涙腺に認められたことから，調節性T細胞の制御異常に加えて，NF-κB2によるT細胞の制御機構に障害をきたすと自己免疫疾患の発症に結びつくことが示された(図7)．

まとめ

Nuclear factor(NF)-κBによる標的遺伝子の転写活性システムはT細胞にとって必須であるといえる．しかし，5つのサブユニットでどれが重要であるのかはいまだ解明されていない．NF-κBのサブユニット遺伝子のそれぞれの欠損マウスの中にはT細胞の分化や末梢トレランスは正常に維持され，T細胞になんらかの刺激が加えられたときにのみ特定の機能に異常が生じている場合がある．また，なんら機能的異常が見出せない場合も報告されている．サブユニットのどれかが欠損しても別のサブユニットが代替的に機能していることも考えられる．実際の免疫反応においてもT細胞にとってNF-κBシグナルに障害が生じれば，別のサブユニットが動員され，過剰なシグナルが伝われば各サブユニットを介して制御的に働くNF-κBネットワークシステムが免疫トレランスの維持に働いているのではなかろうか．今後，NF-κBシグナルと免疫疾患との関係を明らかにすることは臨床的にもきわめて有用であるといえる．

文　献

1) Karin M, Ben-Neriah Y. Phosphorylation meets ubiquitination : the control of NF-κB activity. Annu Rev Immunol 2000 ; 18 : 621.
2) Karin M. How NF-kappaB is activated : the role of the IkappaB kinase (IKK) complex. Oncogene 1999 ; 18 : 6867.
3) Bonizzi G, Karin M. The two NF-kappaB activation pathways and their role in innate and adaptive immunity. Trends Immunol 2004 ; 25 : 280.
4) Kahn-Perles B, Lipcey C, Lecine P, et al. Temporal and subunit-specific modulations of the Rel/NF-kappaB transcription factors through CD28 costimulation. J Biol Chem 1997 ; 272 : 21774.
5) Sun Z, Arendt CW, Ellmeier W, et al. PKC-theta is required for TCR-induced NF-kappaB activation in mature but not immature T lymphocytes. Nature 2000 ; 404 : 402.
6) Lee K, D'Acquisto F, Hyden M, et al. PDK1 nucleates T cell receptor-induced signaling complex for NF-κB activation. Science 2005 ; 308 : 114.
7) Trushin SA, Pennington KN, Algeciras-Schimnich A, et al. Protein kinase C and calcineurin synergize to activate IκB kinase and NF-κB in T lymphocytes. J Biol Chem 1999 ; 274 : 22923.
8) Pimentel-Muinos FX, Mazana J, Fresno M. Regulation of interleukin-2 alpha chain expression and nuclear factor kappa B activation by protein kinase C in T lymphocytes. Autocrine role of tumor necrosis factor alpha. J Biol Chem 1994 ; 269 : 24424.

9) Prasad AS, Bao B, Beck FW, et al. Zinc enhances the expression of interleukin-2 and interleukin-2 receptors in HUT-78 cells by way of NF-kappaB activation. J Lab Clin Med 2002 ; 140 : 272.
10) Rawlings DJ, Sommer K, Moreno-Garcia ME. The CARMA1 signalosome links the signaling machinery of adaptive and annate immunity in lymphocytes. Nat Rev Immunol 2006 ; 6 : 799.
11) Hayden MS, West AP, Ghosh S. NF-κB and immune response. Oncogene 2006 ; 25 : 6758.
12) Novack DV, Yin L, Hagen-Stapleton A, et al. The IkappaB function of NF-kappaB2 p100 controls stimulated osteoclastogenesis. J Exp Med 2003 ; 198 : 771.
13) Weih F, Carrasco D, Durham SK, et al. Multiorgan inflammation and hematopoietic abnormalities in mice with a targeted disruption of RelB, a member of the NF-kappa B/Rel family. Cell 1995 ; 80 : 331.
14) Kajiura F, Sun S, Nomura T, et al. NF-kappa B-inducing kinase establishes self-tolerance in a thymic stroma-dependent manner. J Immunol 2004 ; 172 : 2067.
15) Ishimaru N, Kishimoto H, Hayashi Y, et al. Regulation of naïve T cell function by the NF-κB2 pathway. Nat Immunol 2006 ; 7 : 763.
16) Matsumoto M, Yamada T, Yoshinaga SK, et al. Essential role of NF-kappa B-inducing kinase in T cell activation through the TCR/CD3 pathway. J Immunol 2002 ; 169 : 1151.
17) Speirs K, Lieberman L, Caamano J, et al. Cutting edge : NF-kappa B2 is a negative regulator of dendritic cell function. J Immunol 2004 ; 172 : 752.
18) Artis D, Speirs K, Joyce K, et al. NF-kappa B1 is required for optimal $CD4^+$ Th1 cell development and resistance to *Leishmania major*. J Immunol 2003 ; 170 : 1995.
19) Erdman S, Fox JG, Dangler CA, et al. Typhlocolitis in NF-kappa B-deficient mice. J Immunol 2001 ; 166 : 1443.
20) Hilliard B, Samoilova EB, Liu TS, et al. Experimental autoimmune encephalomyelitis in NF-kappa B-deficient mice : roles of NF-kappa B in the activation and differentiation of autoreactive T cells. J Immunol 1999 ; 163 : 2937.
21) Beg AA, Sha WC, Bronson RT, et al. Embryonic lethality and liver degeneration in mice lacking the RelA component of NF-kappa B. Nature 1995 ; 376 : 167.
22) Doi T, Takahashi T, Taguchi O, et al. NF-κB RelA-deficient lymphocytes : Normal development of T cells and B cells, impaired production of IgA and IgG1 and reduced proliferative responses. J Exp Med 1997 ; 185 : 953.
23) Hilliard BA, Mason N, Xu L, et al. Critical roles of c-Rel in autoimmune inflammation and helper T cell differentiation. J Clin Invest 2002 ; 110 : 843.
24) Franzoso G, Carlson L, Poljak L, et al. Mice deficient in nuclear factor (NF)-kappa B/p52 present with defects in humoral responses, germinal center reactions, and splenic microarchitecture. J Exp Med 1998 ; 187 : 147.
25) Tsubata R, Tsubata T, Hiai H, et al. Autoimmune disease of exocrine organs in immunodeficient alymphoplasia mice : a spontaneous model for Sjogren's syndrome. Eur J Immunol 1996 ; 26 : 2742.
26) Lu L, Gondek DC, Scott ZA, et al. NF-κB-inducing kinase deficiency results in the development of a subset of regulatory T cells, which shows a hyperproliferative activity upon glucocorticoid-induced TNF receptor family-related gene stimulation. J Immunol 2005 ; 175 : 1651.

* * *

Visualizing the dynamics of p21$^{Waf1/Cip1}$ cyclin-dependent kinase inhibitor expression in living animals

Naoko Ohtani*†, Yuko Imamura*, Kimi Yamakoshi*, Fumiko Hirota‡, Rika Nakayama§, Yoshiaki Kubo¶, Naozumi Ishimaru¶, Akiko Takahashi*, Atsushi Hirao‖**, Takatsune Shimizu††, David J. Mann‡‡, Hideyuki Saya††, Yoshio Hayashi¶, Seiji Arase¶, Mitsuru Matsumoto‡, Kazuki Nakao§, and Eiji Hara*†

*Institute for Genome Research, ‡Institute for Enzyme Research, and ¶Institute of Health Biosciences, University of Tokushima, Tokushima 770-8503, Japan; §Center for Developmental Biology, RIKEN, Kobe 650-0047, Japan; ‖Cancer Research Institute, Kanazawa University, Kanazawa 920-0934, Japan; **CREST, Japan Science and Technology Agency, Tokyo 102-0075, Japan; ††Institute for Advanced Medical Research, Keio University School of Medicine, Tokyo 160-8582, Japan; and ‡‡Division of Cell and Molecular Biology, Imperial College London, London SW7 2AZ, United Kingdom

Communicated by Thaddeus P. Dryja, Harvard Medical School, Boston, MA, July 25, 2007 (received for review May 11, 2007)

Although the role of *p21$^{Waf1/Cip1}$* gene expression is well documented in various cell culture studies, its *in vivo* roles are poorly understood. To gain further insight into the role of *p21$^{Waf1/Cip1}$* gene expression *in vivo*, we attempted to visualize the dynamics of *p21$^{Waf1/Cip1}$* gene expression in living animals. In this study, we established a transgenic mice line (p21-*p*-luc) expressing the firefly luciferase under the control of the *p21$^{Waf1/Cip1}$* gene promoter. In conjunction with a noninvasive bioluminescent imaging technique, p21-*p*-luc mice enabled us to monitor the endogenous *p21$^{Waf1/Cip1}$* gene expression *in vivo*. By monitoring and quantifying the *p21$^{Waf1/Cip1}$* gene expression repeatedly in the same mouse throughout its entire lifespan, we were able to unveil the dynamics of *p21$^{Waf1/Cip1}$* gene expression in the aging process. We also applied this system to chemically induced skin carcinogenesis and found that the levels of *p21$^{Waf1/Cip1}$* gene expression rise dramatically in benign skin papillomas, suggesting that *p21$^{Waf1/Cip1}$* plays a preventative role(s) in skin tumor formation. Surprisingly, moreover, we found that the level of *p21$^{Waf1/Cip1}$* expression strikingly increased in the hair bulb and oscillated with a 3-week period correlating with hair follicle cycle progression. Notably, this was accompanied by the expression of p63 but not p53. This approach, together with the analysis of *p21$^{Waf1/Cip1}$* knockout mice, has uncovered a novel role for the *p21$^{Waf1/Cip1}$* gene in hair development. These data illustrate the unique utility of bioluminescence imaging in advancing our understanding of the timing and, hence, likely roles of specific gene expression in higher eukaryotes.

aging | cell cycle | hair cycle | imaging

The founding member of the mammalian cyclin-dependent kinase (CDK) inhibitor family, p21$^{Waf1/Cip1}$, is one of the best characterized transcriptional targets of the p53 tumor suppressor protein (1–4). As a general inhibitor of CDKs, p21$^{Waf1/Cip1}$ prevents phosphorylation of the retinoblastoma tumor suppressor protein (pRb) thereby enhancing its growth suppressive function (2, 3, 5). Thus, p21$^{Waf1/Cip1}$ links the p53 pathway to the pRb pathway, providing a tight security network toward tumor suppression. Indeed, the tumor-suppressive role of p21$^{Waf1/Cip1}$ is well documented in various cell culture studies; up-regulation of the *p21$^{Waf1/Cip1}$* gene expression participates in processes such as DNA damage-induced cell cycle arrest, cellular senescence, and terminal differentiation, each of which may prevent tumor formation (5, 6). However, *in vivo*, the role of p21$^{Waf1/Cip1}$, especially in the context of tumor suppression, remains unclear. For example, mutations in the *p21$^{Waf1/Cip1}$* gene are rarely observed in human cancers (7), and, although the majority of mice lacking the *p53* gene develop spontaneous tumors by 6 months of age (8, 9), mice lacking the *p21$^{Waf1/Cip1}$* gene do not exhibit any predisposition to spontaneous tumor formation (10, 11). These observations raise a question of whether the results seen in cell culture truly reflect the physiological roles of p21$^{Waf1/Cip1}$ *in vivo*. However, because knockout experiments performed to date have used mice with germ-line deficiencies at the *p21$^{Waf1/Cip1}$* gene locus, there is the possibility of developmental compensation, as seen with other cell cycle regulators (12, 13). Moreover, expression of the *p21$^{Waf1/Cip1}$* gene overlaps with that of other CDK inhibitor family members in many different tissues (5). It is, therefore, possible that the effects of *p21$^{Waf1/Cip1}$* deficiency is somewhat compromised by developmental or somatic compensation by functionally related CDK inhibitors in *p21$^{Waf1/Cip1}$* knockout mice. Alternative approaches are therefore needed to supplement the *in vitro* studies and assist in understanding the physiological roles of *p21$^{Waf1/Cip1}$* gene expression *in vivo*.

Bioluminescence imaging (BLI) is an emerging approach that is based on detection of light emission from cells or tissues (14, 15). Optical imaging by bioluminescence allows a noninvasive and real-time analysis of various biological responses, such as gene expression, proteolytic processing, or protein–protein interactions, in living animals (16–20). In this study, we generated a transgenic mice line (p21-*p*-luc) expressing the firefly luciferase under the control of the *p21$^{Waf1/Cip1}$* gene promoter. Using this mouse model, we explored the dynamics of *p21$^{Waf1/Cip1}$* gene expression in many different biological processes *in vivo*. This approach, in conjunction with the analysis of *p21$^{Waf1/Cip1}$* knockout mice, uncovered a previously uncharacterized function of *p21$^{Waf1/Cip1}$* gene expression in hair development. The ability to image *p21$^{Waf1/Cip1}$* gene expression noninvasively therefore provides a valuable tool for studies on the role of *p21$^{Waf1/Cip1}$* gene expression *in vivo*.

Results

To study how *p21$^{Waf1/Cip1}$* gene expression is regulated *in vivo*, we attempted to visualize the transcriptional activity of the *p21$^{Waf1/Cip1}$* gene in living animals. To this end, a transgenic mice line (p21-*p*-luc mice) expressing the firefly luciferase

Author contributions: N.O. and Y.I. contributed equally to this work; N.O. and E.H. designed research; N.O., Y.I., K.Y., F.H., R.N., Y.K., N.I., A.T., A.H., and T.S. performed research; N.O., D.J.M., H.S., Y.H., S.A., M.M., K.N., and E.H. analyzed data; and N.O. and E.H. wrote the paper.

The authors declare no conflict of interest.

Freely available online through the PNAS open access option.

Abbreviations: CDK, cyclin-dependent kinase; pRb, retinoblastoma tumor suppressor protein; BLI, bioluminescence imaging.

†To whom correspondence may be addressed. E-mail: ohtani@genome.tokushima-u.ac.jp or hara@genome.tokushima-u.ac.jp.

This article contains supporting information online at www.pnas.org/cgi/content/full/0706949104/DC1.

www.pnas.org/cgi/doi/10.1073/pnas.0706949104

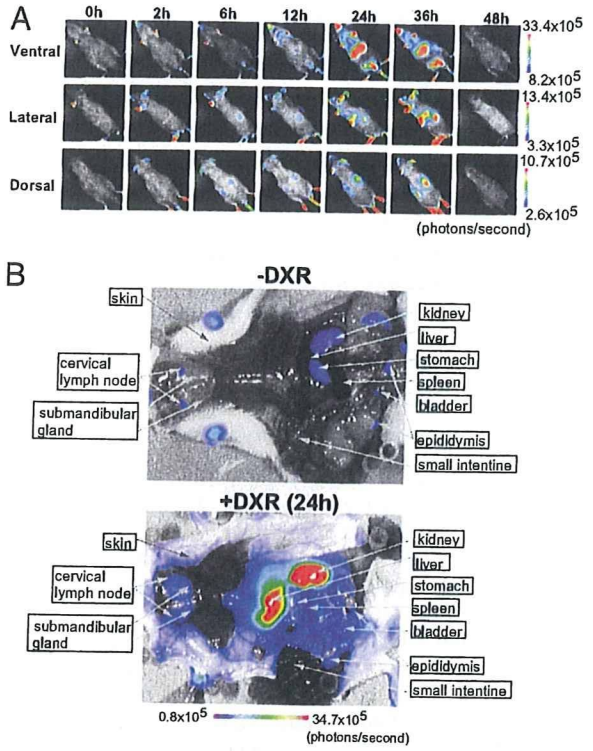

Fig. 1. Characterization of the p21-*p*-luc mice. (*A*) The p21-*p*-luc mice (8-week-old) were injected i.p. with doxorubicin (DXR) (20 mg/kg) and were subjected to noninvasive BLI at various times after doxorubicin (DXR) injection. Representative images of five different experiments are shown. (*B*) The same line of p21-*p*-luc mice were treated with doxorubicin (+DXR) (20 mg/kg) or saline (−DXR) for 24 h, injected with luciferin, and incised through the mouth and anus under anesthesia. Representative BLI data of five different experiments are shown. The color bar indicates photons with minimum and maximum threshold values.

driven by the $p21^{Waf1/Cip1}$ gene promoter, which contains two p53-binding sites, was established and subjected to noninvasive *in vivo* BLI. Although basal levels of bioluminescent signals were very low throughout the body, except for the paws, a striking increase in signal was observed (particularly over the abdomen) within 24 h of treatment with doxorubicin, a DNA damaging agent that activates p53 (Fig. 1*A*). These signals were sustained until 36 h and then declined to baseline values within the next 12 h (Fig. 1*A*, 48 h). To define the organs expressing high levels of luciferase activity, the same lines of transgenic mice were treated with or without doxorubicin for 24 h, injected with luciferin, and incised through mouth and anus under anesthesia (Fig. 1*B*). As expected from noninvasive BLI data (Fig. 1*A*, 24 h), a significant induction of bioluminescent signal was observed in liver and kidney in doxorubicin-treated mice [Fig. 1*B* and supporting information (SI) Fig. 4*A*]. A substantial but less pronounced induction was observed in the submandibular gland, spleen, bladder, and stomach (Fig. 1*B* and SI Fig. 4*A*). Similar but different dynamics of $p21^{Waf1/Cip1}$ gene expression was observed by x-ray irradiation (SI Fig. 5). Importantly, the levels of bioluminescent signal were well correlated with those of endogenous $p21^{Waf1/Cip1}$ mRNA (SI Figs. 4 and 5), indicating that, in the p21-*p*-luc mice, luciferase expression accurately reports the transcriptional dynamics of $p21^{Waf1/Cip1}$ gene expression *in vivo*. Furthermore, in concordance with the levels of endogenous $p21^{Waf1/Cip1}$ expression, luciferase activity was strikingly increased in the cortex and medulla of the kidney (SI Fig. 6). Taken together, these results suggest that the p21-*p*-luc mice provide an ideal tool for the analysis of $p21^{Waf1/Cip1}$ gene expression *in vivo*.

Although p53 serves the beneficial function of tumor suppression, p53 activation may, in some circumstance, act in a manner detrimental to the long-term homeostasis of living organism (21). Indeed, aberrant activation of p53 is known to accelerate the aging process in mice, and the induction of $p21^{Waf1/Cip1}$ gene expression has been shown to be involved this process (22, 23). We thus next attempted to explore the dynamics of $p21^{Waf1/Cip1}$ gene expression throughout entire life span in p21-*p*-luc mice (SI Fig. 7). Unexpectedly, only a slight (3- to 4-fold) induction of bioluminescent signal was observed in aged kidney but not in other aged organs or tissues (SI Fig. 7). Surprisingly, moreover, any signs of strong activation of p53 and DNA damage responses were not observed in aged kidney (SI Fig. 7), indicating that the induction of $p21^{Waf1/Cip1}$ gene expression in aged kidney is likely to be regulated by a p53-independent mechanism, although we cannot rule out the possibility that weak activation of p53 contributes to the up-regulation of $p21^{Waf1/Cip1}$ gene expression.

The up-regulation of $p21^{Waf1/Cip1}$ gene expression is implicated in cellular senescence, the state of stable cell cycle arrest provoked by diverse stresses including DNA damage and oncogenic *ras* expression in cultured primary cells (4, 24). To explore this notion *in vivo*, p21-*p*-luc mice were subjected to a conventional chemically induced skin tumor protocol with a single dose of DMBA for initiation and biweekly treatment with 12-*o*-tetradecanoylphorbol 13-acetate (TPA) for promotion. Because this protocol causes an oncogenic mutation in the H-*ras* gene, it appeared to be ideal for studying physiological responses against oncogenic *ras* expression in living animals (25, 26). In agreement with previous reports (25, 26), benign skin papillomas began to appear after 7–8 weeks of promotion (Fig. 2*A*). Notably, papilloma formation was accompanied by the induction of a bioluminescence signal (Fig. 2*A*), endogenous $p21^{Waf1/Cip1}$ expression, and activation of p53 (Fig. 2*B*). These observations, together with previous studies that indicate that disruption of the $p21^{Waf1/Cip1}$ gene results in an increase of papilloma formation or carcinoma formation (27–29), strongly suggest that $p21^{Waf1/Cip1}$ plays a preventative role against oncogenic *ras*-signaling *in vivo*.

Because noninvasive BLI permits continuous readout of gene expression in living animals (14, 15), we next examined the kinetics of $p21^{Waf1/Cip1}$ gene expression toward papilloma formation. To our surprise, a remarkable bioluminescent signal was observed well before papilloma appearance and oscillated with a 3-week period (Figs. 2 *C* and *D*). Unexpectedly, moreover, a remarkable expression of endogenous $p21^{Waf1/Cip1}$ was observed in the hair bulb, but not in the skin itself (Fig. 2*E*), suggesting that $p21^{Waf1/Cip1}$ may play a role in hair development. To produce new hairs, existing hair follicles undergo cycles of growth (anagen), regression (catagen), and rest (telogen) (30). Because TPA treatment has been shown to promote entry of hair follicles into their anagen phase (31), we next asked whether the oscillating bioluminescence signal in DMBA/TPA-treated skin reflects hair follicle cycle progression. Although TPA treatment, in itself, did not cause skin papilloma formation, a similar oscillation of bioluminescence signals and $p21^{Waf1/Cip1}$ mRNA expression was induced by TPA treatment alone (SI Fig. 8). Notably, this was accompanied by remarkable hair growth (SI Fig. 8*A*), suggesting a role for $p21^{Waf1/Cip1}$ in the hair follicle cycle progression in mouse skin.

To substantiate this idea in a more physiological setting, we next tested whether $p21^{Waf1/Cip1}$ expression oscillates throughout the natural hair follicle cycle, exploiting the fact that hair follicle cycles are synchronized for the first two postnatal periods of hair follicle growth in mice (32). Although the dynamics of hair cycle progression were visually undetectable during the second postnatal hair follicle cycle, BLI was sensitive enough to monitor oscillating $p21^{Waf1/Cip1}$ expression (Fig. 3*A*). The levels of biolu-

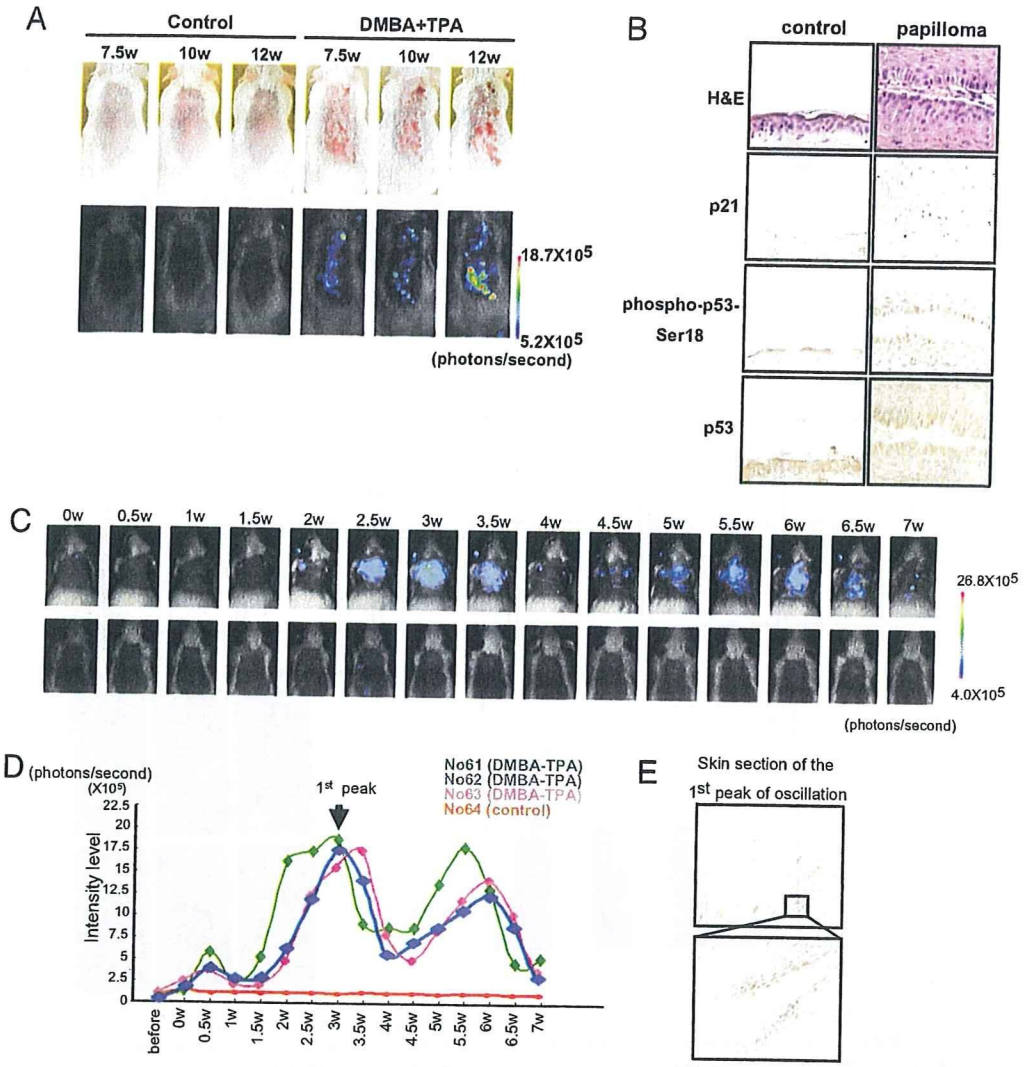

Fig. 2. Oscillation of bioluminescence signals in DMBA/TPA-treated mouse skin. (*A*) The p21-*p*-luc mice treated with DMBA/TPA or with acetone (control) were subjected to noninvasive BLI at indicated time points after TPA treatment. Representative images of 12 different experiments were shown (*Lower*). These papillomas and control skin were photographed in regular lighting (*Upper*). The color bar indicates photons with minimum and maximum threshold values. (*B*) H&E staining and the immunohistochemistry for endogenous $p21^{Waf1/Cip1}$ expression, phosphorylation of p53 at serine 18 residue, and p53 expression were performed by using biopsy samples of skin papilloma (*Right*) or control normal skin (*Left*). (*C*) Noninvasive BLI was performed throughout the time course after DMBA/TPA treatment (*Upper*) or acetone control (*Lower*). Mice were imaged at 0.5-week intervals after TPA treatment. Representative images of 12 different experiments were shown. The color bar indicates photons with minimum and maximum threshold values. (*D*) The intensity of bioluminescence signal throughout the time course was graphed. (*E*) Immunohistochemistry was conducted to examine the endogenous $p21^{Waf1/Cip1}$ expression in the dorsal skin at 3 weeks after TPA treatment (corresponding to the first peak of bioluminescence oscillation). A magnified image of hair bulb is shown (*Lower*).

minescence signals reached their peak at postnatal day 28 (P28); endogenous $p21^{Waf1/Cip1}$ expression was also strongly observed in the precortex area above the hair matrix (differentiating cell area) at this time (Fig. 3*A*). These data suggest that $p21^{Waf1/Cip1}$ may regulate the size of hair bulb and thereby control the hair phenotype.

To explore this possibility, microscopic examination of the various hair types was conducted by using mice with different $p21^{Waf1/Cip1}$ genotypes (10). The morphology of the four main hair types (guard, awl, auchene, and zigzag) was not significantly different among three different genotypes ($p21^{+/+}$, $p21^{+/-}$, $p21^{-/-}$) (data not shown). However, the proportion of zigzag hairs, which are produced by the smallest hair bulb, was significantly reduced in $p21^{+/-}$ mice, whereas awl hairs and auchene hairs, which are produced by the intermediate-sized hair bulb, were increased (Fig. 3*B*). Curiously, these effects were less pronounced in $p21^{-/-}$ mice (Fig. 3*B*). Importantly, however, unusually high level of $p27^{Kip1}$ expression, another member of the $p21^{Waf1/Cip1}$ family CDK inhibitors, was observed in the hair bulb of $p21^{-/-}$ mice (Fig. 3*C*). Thus, it is likely that the effects of $p21^{Waf1/Cip1}$ deficiency are concealed, at least in part, by up-regulation of $p27^{Kip1}$ expression in the hair bulb of $p21^{-/-}$ mice. In line with this observation, the proportion of zigzag hairs has been shown to reduce in $p27^{Kip1}$ knockout mice (33), suggesting that $p21^{Waf1/Cip1}$ and $p27^{Kip1}$ possess overlapping role(s) in hair development.

It is worthwhile to note that a similar level of $p21^{Waf1/Cip1}$ expression was observed in anagen hair bulbs, regardless of p53 gene status (SI Fig. 9*A*). Moreover, the proportion of four main hair types was not substantially different among mice of three different genotypes ($p53^{+/+}$, $p53^{+/-}$, $p53^{-/-}$) (SI Fig. 9*B*), suggesting that p53 is not a major player in this setting. Interestingly, although we were unable to see any p53 expression in the hair bulb throughout hair follicle cycle (data not shown), the levels of

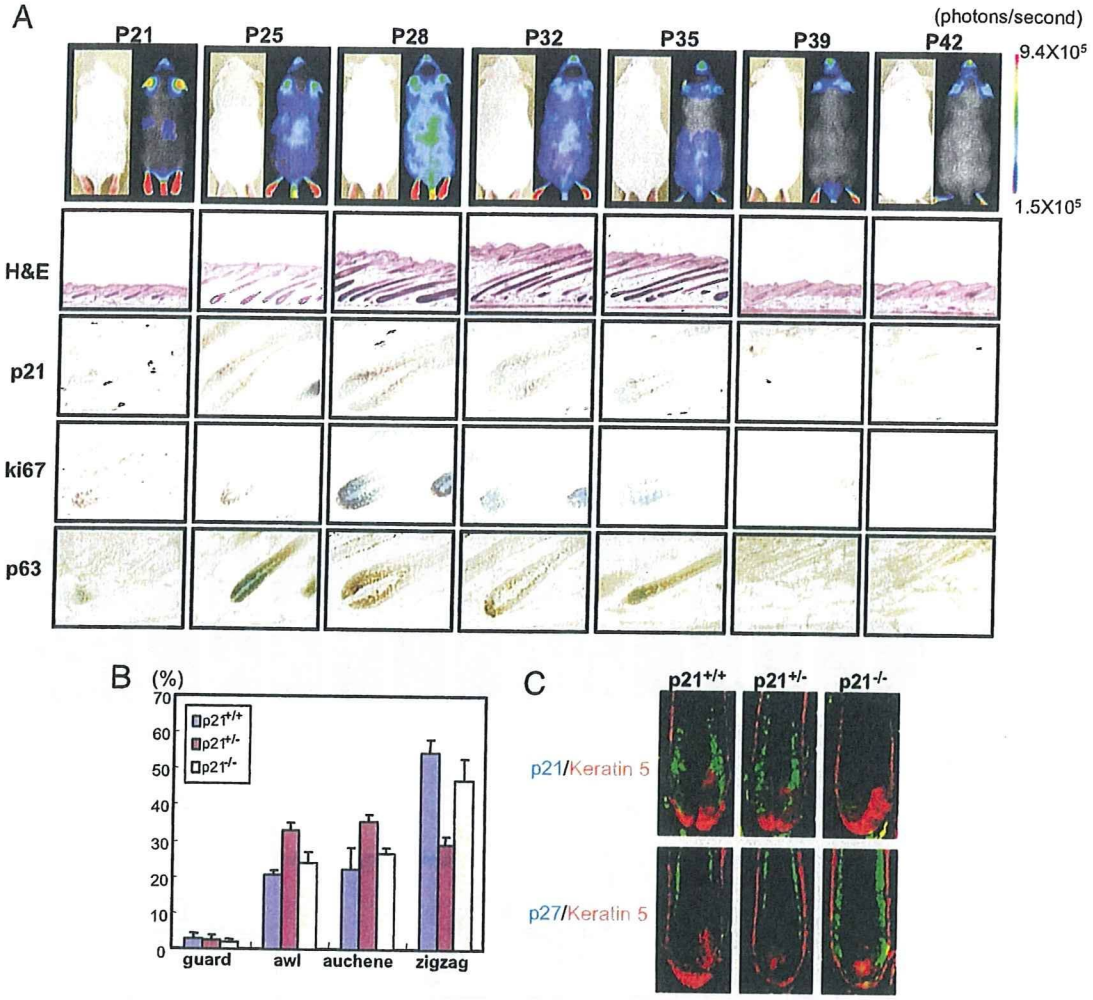

Fig. 3. Real-time imaging of hair follicle cycle oscillation in living mice. (*A*) The p21-*p*-luc mice were subjected to noninvasive BLI from postnatal day 21 (P21) to P42. Representative images of five different experiments are shown at the top. The color bar indicates photons with minimum and maximum threshold values. At the indicated time point of postnatal development, dorsal skin of p21-*p*-luc mice was harvested and processed for H&E staining or for immunohistochemistry. (*B*) Summary of the prevalence of hair phenotypes in mice of different $p21^{Waf1/Cip1}$ genotype (C57BL/6 background). The means ± SD of three independent experiments are shown. (*C*) Immunofluorescence of dorsal skin section from P28 mice was performed by using antibodies against $p21^{Waf1/Cip1}$ (green) or $p27^{Kip1}$ (green). Keratin 5 (red) was used as a marker for outer root sheath.

p63 (34), a member of p53-family of transcription factors, were dramatically increased in anagen hair bulbs (Fig. 3*A*). Together, these results imply that p63, but not p53, may play a critical role in the regulation of hair development.

Discussion

In this study, we generated a transgenic mouse model to visualize $p21^{Waf1/Cip1}$ gene expression in living animals. The p21-*p*-luc mice carry the firefly luciferase cDNA under the control of the $p21^{Waf1/Cip1}$ gene promoter. Because this promoter contains two canonical p53-binding sites, this mouse model is expected to be an ideal system for monitoring not only $p21^{Waf1/Cip1}$ gene expression, but also p53 activation *in vivo*. Indeed, a dramatic induction of bioluminescent signal was observed in various organs within 24 h upon treatment with doxorubicin, a well known DNA-damaging agent that activates p53 (Fig. 1 and SI Fig. 4). Notably, different dynamics of $p21^{Waf1/Cip1}$ gene expression were observed when p21-*p*-luc mice were irradiated with x-ray (SI Fig. 5). In both cases, the levels of bioluminescent signals observed were well correlated with those of endogenous $p21^{Waf1/Cip1}$ mRNA detected by RT-PCR analysis (Fig. 1 and SI Figs. 4 and 5), indicating that the p21-*p*-luc mice provide an ideal tool to monitor the expression of $p21^{Waf1/Cip1}$ gene and/or activity of p53 in living animals. Interestingly, neither doxorubicin nor x-rays induced $p21^{Waf1/Cip1}$ gene expression in the small intestine, implying that p53 is not a major regulator of $p21^{Waf1/Cip1}$ gene expression in the small intestine, as suggested by previous studies (35).

By monitoring and quantifying $p21^{Waf1/Cip1}$ gene expression repeatedly in the same mouse throughout its entire life span, we revealed the dynamics of $p21^{Waf1/Cip1}$ gene expression during the aging process in living mice. Only a slight (3- to 4-fold) induction of bioluminescent signal was observed in kidney, but not in other organs, as mice age (SI Fig. 7). Moreover, strong signs of p53 activation and DNA damage responses were virtually undetectable in aged kidney (SI Fig. 7). These results were unexpected because several lines of evidence suggest that p53-dependent induction of $p21^{Cip1/Waf1}$ is involved in the aging process (22, 23, 36). Our results are, however, consistent with a recent RT-PCR-based study showing that only a slight increase in the $p21^{Waf1/Cip1}$ gene expression was seen in tissues from old mice versus young mice (37, 38). Moreover, it has been shown that increased p53 expression under the endogenous p53 gene promoter protects mice from tumorigenesis without showing any indication of

accelerated aging (39). Furthermore, $p21^{Waf1/Cip1}$ appears to play protective effects on stem cell exhaustion and ionizing radiation, which may underlie the long-term homeostasis throughout entire life span (40–42). Thus, it is likely that the role of $p21^{Waf1/Cip1}$ in organismal aging is context-dependent and more complicated than envisaged.

Another important aspect of the $p53/p21^{Waf1/Cip1}$ pathway is the induction of cellular senescence (4, 24), the state of permanent cell cycle arrest provoked by a variety of oncogenic stimuli including oncogenic *ras* expression in cultured primary cells (43–45). Because this mechanism is poorly understood *in vivo* (46), we tested this notion using our *in vivo* BLI system. Indeed, DMBA/TPA treatment, which causes an oncogenic mutation of the endogenous H-*ras* gene (25, 26), resulted in a significant induction of $p21^{Waf1/Cip1}$ expression accompanied by skin papilloma formation (Fig. 2*A*). Because the induction of $p21^{Waf1/Cip1}$ expression can be seen from the very beginning of papilloma formation and was further enhanced as the papillomas developed (Fig. 2*A*), the $p21^{Waf1/Cip1}$ gene is likely to play multiple roles in preventing benign skin papilloma formation and/or malignant conversion. These results are somewhat consistent with two conflicting reports; one shows that disruption of the $p21^{Waf1/Cip1}$ gene accelerates benign skin papilloma formation but not malignant conversion (27), and the other shows that disruption of the $p21^{Waf1/Cip1}$ gene accelerates malignant conversion but not benign skin papilloma formation (28).

During the time-course BLI experiments in skin tumor formation, we unexpectedly found that the expression of $p21^{Waf1/Cip1}$ oscillates over the 3-week time course of the hair follicle cycle (Figs. 2 *C* and *D* and 3*A*). Moreover, although the morphology of the four main hair types was not remarkably different, the proportion of zigzag hairs, which are produced by the smallest hair bulb, was significantly reduced in $p21^{+/-}$ mice (Fig. 3*B*). Surprisingly, the effects of $p21^{Waf1/Cip1}$ deficiency were less pronounced in $p21^{-/-}$ mice than in heterozygotes (Fig. 3*B*) because of an up-regulation of $p27^{Kip1}$ expression in the hair bulb of $p21^{-/-}$ mice (Fig. 3*C*). In concordance with this notion, recent study revealed that the proportion of zigzag hairs is substantially reduced in mice lacking $p27^{Kip1}$ (33) Thus, there is cross-talk between $p21^{Waf1/Cip1}$ and $p27^{Kip1}$ in controlling hair phenotype. Note that the proportion of zigzag hairs is also reduced in mice lacking the *Sox18* gene (47), and Sox family transcription factors are known to activate $p21^{Waf1/Cip1}$ expression (48). Thus, it is tempting to speculate that Sox18 controls hair phenotype through regulating $p21^{Waf1/Cip1}$ gene expression in the hair bulb. It is also important to note, however, that the expression of p63 (34), a member of p53 family transcription factor, overlapped with that of $p21^{Waf1/Cip1}$ in the hair bulb (Fig. 3*A*). It is therefore likely that $p21^{Waf1/Cip1}$ gene expression is controlled by multiple factors in hair bulbs.

We are currently uncertain about the biological consequence of alteration of the zigzag hair proportion in $p21^{+/-}$ mice. However, because the hair coat plays a crucial role in controlling body temperature in the wild, it is interesting to speculate that $p21^{Waf1/Cip1}$ and/or $p27^{Kip1}$ may be involved in temperature control in the wild. Taken together, our results reveal an unexpected role for $p21^{Waf1/Cip1}$ and provide an insight into how the hair phenotype is determined. Visualizing the dynamics of $p21^{Waf1/Cip1}$ gene expression in living mice, therefore, provides a powerful tool for not only help to resolve and clarify issues connecting *in vitro* studies but also reveals unrecognized functions of this key proliferative regulator in various physiological processes *in vivo*.

Materials and Methods

Generation of p21-*p*-luc transgenic mouse. The 2.5-kb fragment of the $p21^{Waf1/Cip1}$ gene promoter containing two p53-binding sites (GenBank accession number: NW_923073.1; from 9663447 to 9665888) was placed in front of the firefly luciferase reporter cDNA in the pGL3-basic plasmid vector (Promega, Madison, WI) (see plasmid construction map in SI Fig. 10). The plasmid DNA was digested with XhoI and SalI, and the DNA fragment containing the $p21^{Waf1/Cip1}$ gene promoter, luciferase cDNA, and polyA signal was isolated and used for microinjection. The transgenic mouse strain was generated by pronuclear microinjection of the reporter transgene into fertilized CD1 oocytes. Genotyping of transgenic mice was determined by PCR and was confirmed by whole-body BLI. One transgenic line, #34 (CDB0415T-34), was selected for studies described in this article because the levels of bioluminescence signals were well correlated with those of endogenous $p21^{Waf1/Cip1}$ mRNA. All animals were cared for by using protocols approved by the Committee for the Use and Care of Animals of the University of Tokushima.

Bioluminescence Imaging. For the detection of luciferase expression, mice were anesthetized, injected i.p. with D-luciferin sodium salt (75 mg/kg) 5 min before beginning photon recording (16–20). Mice were placed in the light-tight chamber, and a gray-scale image of the mice was first recorded with dimmed light, followed by acquisition of luminescence image by using a cooled CCD camera (Princeton Instruments, Trenton, NJ). The signal-to-noise ratio was increased by 2 × 2 binning and 5 min exposure, unless otherwise stated in the text. For colocalization of the luminescent photon emission on the animal body, gray scale and pseudocolor images were merged by using IMAGE-PRO PLUS (Media Cybernetics, Bethesda, MD).

Tumor-Induction Experiments. Twelve mice of the p21-*p*-luc line, in the resting phase of the hair cycle (8-week-old), were shaved and treated with 7,12-dimethylbenzanthracene (DMBA) (100 μg in 100 μl of acetone). One week after DMBA treatment, mice were subsequently treated twice a week with TPA (12.5 μg in 100 μl of acetone) for 20 weeks (25, 26). Control mice were treated with acetone instead of DMBA/TPA.

Semiquantitative RT-PCR. Total RNA was isolated by using TRIzol reagent (Invitrogen, Carlsbad, CA), and 2 μg of total RNA was used for the reverse-transcriptase reaction. The PCR was performed by using Blend Taq polymerase (TOYOBO, Osaka, Japan) with primers specific for the mouse $p21^{Waf1/Cip1}$ gene and the mouse *β-actin* gene. The PCR primer sequences used are shown in *SI Text*.

Real-Time RT-PCR. Quantitative real-time RT-PCR was performed by using the SYBER Premix EX Taq system (TAKARA, Otsu, Japan) and an ABI Prism 7900HT (Applied Biosystems, Foster City, CA). Amplified signals were confirmed to be single bands by gel electrophoresis and were normalized to the levels of GAPDH. Data were analyzed by using SDS2.1 software (Applied Biosystems). The PCR primer sequences used are shown in *SI Text*.

Histology and Immunohistochemistry. Biopsies of mouse skin taken from the middorsal region were fixed in 10% formalin for a 24 h or longer, progressively dehydrated through gradients of alcohol, and embedded in paraffin. Samples were sectioned on a microtome (5-μm-thick), deparaffinized in xylene, rehydrated, and then stained with hematoxylin and eosin (H&E). The hair cycle status was determined by histological examination. For antibody staining, deparaffinized and rehydrated sections were exposed to heat-induced antigen retrieval for 5 min or 20 min in 10 mM citrate buffer (pH 6.0). After washing in PBS, endogenous peroxidase activity was quenched for 15 min in 1% H_2O_2 in methanol, followed by washing with PBS. The sections were

incubated in blocking serum for 1 h at room temperature. After incubation with primary antibodies overnight at 4°C, biotinylated anti-mouse secondary antibody was applied and detected by the avidin–biotin peroxidase technique using the DAB kit (DAKO, Glostrup, Denmark) and then counterstained with methyl green. For immunofluorescence, the relevant Alexa Fluor 488 goat anti-mouse or 546 goat anti-rabbit antibodies (1:1,000; Invitrogen) were used for detection of primary antibodies. Fluorescence images were observed and photographed by using an immunofluorescence microscope (Carl Zeiss, Oberkochen, Germany). The primary antibodies used are shown in *SI Text*.

Hair Measurements. Hair was removed from the middorsal region of each mouse (8-week-old) to reduce the potential regional variation, although this is not known to occur in the dorsal region of the mouse. One hundred hairs were examined to determine the percentage of each hair type.

We thank Dr. P. Leder (Department of Genetics, Harvard Medical School, Boston, MA) for providing $p21^{Waf1/Cip1}$ knockout mice. We also thank Ms. S. Chiba for her assistance in various mouse experiments. This work was supported by grants from Ministry of Education, Science, Sports, and Culture of Japan, the Astellas Foundation for Research on Metabolic Disorders and the Astellas Foundation for Research on Medical Resources.

1. El-Deiry WS, Tokino T, Velculescu VE, Levy DB, Parsons R, Trent JM, Lin D, Mercer WE, Kinzler KW, Vogelstein B (1993) *Cell* 75:817–825.
2. Harper JW, Adami GR, Wei N, Keyomarsi K, Elledge SJ (1993) *Cell* 75:805–816.
3. Xiong Y, Hannon GJ, Zhang H, Casso D, Kobayashi R, Beach D (1993) *Nature* 366:701–704.
4. Noda A, Ning Y, Venable SF, Pereira-Smith OM, Smith JR (1994) *Exp Cell Res* 211:90–98.
5. Sherr CJ, Roberts JM (1999) *Genes Dev* 13:1501–1512.
6. Rowland BD, Peeper DS (2006) *Nat Rev Cancer* 6:11–23.
7. El-Deiry WS (1998) *Curr Top Microbiol Immunol* 227:121–137.
8. Donehower LA, Harvey M, Slagle BL, McArthur MJ, Montgomery CA, Jr, Butel JS, Bradley A (1992) *Nature* 356:215–221.
9. Jacks T, Remington L, Williams BO, Schmitt EM, Halachmi S, Bronson RT, Weinberg RA (1994) *Curr Biol* 4:1–7.
10. Deng C, Zhang P, Harper JW, Elledge SJ, Leder P (1995) *Cell* 82:675–684.
11. Brugarolas J, Chandrasekaran C, Gordon JI, Beach D, Jacks T, Hannon GJ (1995) *Nature* 377:552–557.
12. Sage J, Mulligan GJ, Attardi LD, Miller A, Chen S, Williams B, Theodorou E, Jacks T (2000) *Genes Dev* 14:3037–3050.
13. Ciemerych MA, Kenney AM, Sicinska E, Kalaszczynska I, Bronson RT, Rowitch DH, Gardner H, Sicinski P (2002) *Genes Dev* 16:3277–3289.
14. Contag PR, Olomu IN, Stevenson DK, Contag CH (1998) *Nat Med* 4:245–247.
15. Gross S, Piwnica-Worms D (2005) *Cancer Cell* 7:5–15.
16. Uhrbom L, Nerio E, Holland EC (2004) *Nat Med* 10:1257–1260.
17. Zhang GJ, Safran M, Wei W, Sorensen E, Lassota P, Zhelev N, Neuberg DS, Shapiro G, Kaelin WG, Jr (2004) *Nat Med* 10:643–648.
18. Li F, Sonveaux P, Rabbani ZN, Liu S, Yan B, Huang Q, Vujaskovic Z, Dewhirst MW, Li CY (2007) *Mol Cell* 26:63–74.
19. Vooijs M, Jonkers J, Lyons S, Berns A (2002) *Cancer Res* 62:1862–1867.
20. Paulmurugan R, Umezawa Y, Gambhir SS (2002) *Proc Natl Acad Sci USA* 99:15608–15613.
21. Sharpless NE, DePinho RA (2002) *Cell* 110:9–12.
22. Tyner SD, Venkatachalam S, Choi J, Jones S, Ghebranious N, Igelmann H, Lu X, Soron G, Cooper B, Brayton C, *et al.* (2002) *Nature* 415:45–53.
23. Maier B, Gluba W, Bernier B, Turner T, Mohammad K, Guise T, Sutherland A, Thorner M, Scrable H (2004) *Genes Dev* 18:306–319.
24. Serrano M, Lin AW, McCurrach ME, Beach D, Lowe SW (1997) *Cell* 88:593–602.
25. Quintanilla M, Brown K, Ramsden M, Balmain A (1986) *Nature* 322:78–80.
26. Kemp CJ (2005) *Semin Cancer Biol* 15:460–473.
27. Weinberg WC, Fernandez-Salas E, Morgan DL, Shalizi A, Mirosh E, Stanulis E, Deng C, Hennings H, Yuspa SH (1999) *Cancer Res* 59:2050–2054.
28. Topley GI, Okuyama R, Gonzales JG, Conti C, Dotto GP (1999) *Proc Natl Acad Sci USA* 96:9089–9094.
29. Oskarsson T, Essers MA, Dubois N, Offner S, Dubey C, Roger C, Metzger D, Chambon P, Hummler E, Beard P, Trumpp A (2006) *Genes Dev* 20:2024–2029.
30. Fuchs E (2007) *Nature* 445:834–842.
31. Flores I, Cayuela ML, Blasco MA (2005) *Science* 309:1253–1256.
32. Sarin KY, Cheung P, Gilison D, Lee E, Tennen RI, Wang E, Artandi MK, Oro AE, Artandi SE (2005) *Nature* 436:1048–1052.
33. Sharov AA, Sharova TY, Mardaryev AN, Tommasi di Vignano A, Atoyan R, Weiner L, Yang S, Brissette JL, Dotto GP, Botchkarev VA (2006) *Proc Natl Acad Sci USA* 103:18166–18171.
34. Senoo M, Pinto F, Crum CP, McKeon F (2007) *Cell* 129:523–536.
35. Macleod KF, Sherry N, Hannon G, Beach D, Tokino T, Kinzler K, Vogelstein B, Jacks T (1995) *Genes Dev* 9:935–944.
36. Choudhury AR, Ju Z, Djojosubroto MW, Schienke A, Lechel A, Schaetzlein S, Jiang H, Stepczynska A, Wang C, Buer J, *et al.* (2007) *Nat Genet* 39:99–105.
37. Krishnamurthy J, Torrice C, Ramsey MR, Kovalev GI, Al-Regaiey K, Su L, Sharpless NE (2004) *J Clin Invest* 114:1299–1307.
38. Edwards MG, Anderson RM, Yuan M, Kendziorski CM, Weindruch R, Prolla TA (2007) *BMC Genomics* 8:80.
39. Garcia-Cao I, Garcia-Cao M, Martin-Caballero J, Criado LM, Klatt P, Flores JM, Weill JC, Blasco MA, Serrano M (2002) *EMBO J* 21:6225–6235.
40. Cheng T, Rodrigues N, Shen H, Yang Y, Dombkowski D, Sykes M, Scadden DT (2000) *Science* 287:1804–1808.
41. Kippin TE, Martens DJ, van der Kooy D (2005) *Genes Dev* 19:756–767.
42. Wang YA, Elson A, Leder P (1997) *Proc Natl Acad Sci USA* 94:14590–14595.
43. Gil J, Peters G (2006) *Nat Rev Mol Cell Biol* 7:667–677.
44. Campisi J (2005) *Cell* 120:513–522.
45. Takahashi A, Ohtani N, Yamakoshi K, Iida S, Tahara H, Nakayama K, Nakayama KI, Ide T, Saya H, Hara E (2006) *Nat Cell Biol* 8:1291–1297.
46. Narita M, Lowe SW (2005) *Nat Med* 11:920–922.
47. Pennisi D, Bowles J, Nagy A, Muscat G, Koopman P (2000) *Mol Cell Biol* 20:9331–9336.
48. Panda DK, Miao D, Lefebvre V, Hendy GN, Goltzman D (2001) *J Biol Chem* 276:41229–41236.